

Revised estimates of CMB B -mode polarization induced by patchy reionization

Anirban Roy,^{a,b,j} Girish Kulkarni,^{c,d,e} P. Daniel Meerburg,^{d,f}
Anthony Challinor,^{c,d,g} Carlo Baccigalupi,^{a,b,h,i} Andrea Lapi,^{a,b,h,i} and
Martin G. Haehnelt^{c,d}

^aSISSA, Via Bonomea 265, 34136 Trieste, Italy

^bInstitute for Fundamental Physics of the Universe (IFPU), Via Beirut 2, 34014 Trieste, Italy

^cInstitute of Astronomy, University of Cambridge, Madingley Road, Cambridge CB3 0HA, UK

^dKavli Institute of Cosmology, University of Cambridge, Madingley Road, Cambridge CB3 0HA, UK

^eTata Institute of Fundamental Research, Homi Bhabha Road, Mumbai 400005, India

^fVan Swinderen Institute for Particle Physics and Gravity, University of Groningen, Nijenborgh 4, 9747 AG Groningen, The Netherlands

^gDAMTP, Centre for Mathematical Sciences, University of Cambridge, Wilberforce Road, Cambridge CB3 0WA, UK

^hINFN-Sezione di Trieste, via Valerio 2, 34127 Trieste, Italy

ⁱINAF-Osservatorio Astronomico di Trieste, via Tiepolo 11, 34131 Trieste, Italy

^jDepartment of Astronomy, Cornell University, Ithaca, NY 14853, USA

E-mail: ar689@cornell.edu

Abstract. The search for primordial gravitational waves through the B -mode polarization pattern in the CMB is one of the major goals of current and future CMB experiments. Besides foregrounds, a potential hurdle in this search is the anisotropic secondary B -mode polarization generated by the scattering of CMB photons off free electrons produced during patchy cosmological reionization. Robust predictions of these secondary anisotropies are challenging because of uncertainties in the reionization history. In this paper, we revise estimates of the reionization-induced B -mode signal by incorporating recent advances in the understanding of reionization through observations of the Lyman- α forest. To derive these B -mode estimates, we use high-dynamic-range radiative transfer simulations of reionization that are calibrated to the Ly α data. These simulations are also consistent with a variety of other high-redshift observations. We find that around multipoles $\ell \approx 100$, reionization induces B -mode power with $\ell(\ell + 1)C_\ell^{BB}/2\pi \approx 4 \times 10^{-6} \mu\text{K}^2$. This secondary signal is thus at the level of the primordial signal with the tensor-to-scalar ratio $r < 10^{-4}$, and can increase by a factor of ~ 50 if reionization is sourced by highly clustered sources residing in haloes with mass of $\sim 10^{11} M_\odot$. Our findings suggest that the contribution of patchy reionization to the search for primordial gravitational waves is unlikely to be a concern for currently planned CMB experiments.

Keywords: reionization – gravitational waves and CMBR polarization – CMBR experiments

ArXiv ePrint: —

Contents

1	Introduction	1
2	Secondary B-mode anisotropies from reionization	3
2.1	B -mode signal due to scattering of the CMB temperature quadrupole	4
2.2	B -mode signal due to patchy screening	4
3	Reionization model calibrated to Lyman-α forest data	5
4	Results	9
4.1	Power spectrum of secondary B -mode anisotropies	9
4.2	Effect of reionization history	12
4.3	Minimum mass of reionization sources	13
4.4	Constraints on the tensor-to-scalar ratio	14
5	Discussion	17

1 Introduction

An important goal for current and next-generation CMB experiments is the detection of B -mode polarization of the CMB induced by primordial gravitational waves [1]. These include the BICEP Array [2], SPT-3G [3], Simons Observatory [4], CMB-S4 [5], LiteBIRD [6], and proposed space missions such as PICO [7], and CMB-Bharat [8]. These experiments hope to build on the successes of past experiments, such as Planck [9], ACT [10], SPT [11], BICEP2/Keck [12] either to detect or significantly reduce the upper limit on the tensor-to-scalar ratio parameter r , which quantifies the relative power in primordial gravitational waves compared to curvature fluctuations, by one or two orders of magnitude from the current limit $r < 0.06$ (95% confidence) [13]. A rather natural target is $r \sim 10^{-3}$ for single-field, slow-roll inflation. It has been argued that models that naturally explain the measured tilt of the power spectrum of primordial curvature fluctuations fall into two classes [14, 15]: one in which the potential driving inflation is a monomial; and one in which the inflaton field is rolling off a plateau with a potential that varies over some characteristic scale. Models in the former class generally produce significant primordial gravitational waves and current limits on r rule out many examples. In the latter case, $r \lesssim 10^{-3}$ corresponds to models where the characteristic scale is below the Planck scale. Detection of primordial B modes would significantly strengthen the evidence for inflation while providing a measurement of the energy scale at which inflation occurred and pointers to how inflation is realised in fundamental theory.

In order to succeed, these experiments will have to confront foreground B -mode polarization. The dominant part of these foregrounds is created by polarized diffuse synchrotron and dust emission from the Galaxy [16], which can be handled by means of avoidance and/or removal strategies [16–18]. Foregrounds with respect to the primary signal from inflation also consist of secondary B -mode polarization anisotropies that can potentially have a significantly larger amplitude than primordial B modes. These include secondary B modes induced by gravitational lensing [19, 20], the thermal and kinetic Sunyaev-Zel’dovich effect [21, 22], and by fluctuations in the Thomson scattering opacity of the Universe during the epoch of reionization [23–27]. Lensing-induced B modes have now been detected by several experiments [11, 28–32]. While this signal can dominate over the primordial B modes on all but the largest scales for $r \lesssim 10^{-2}$, it is possible to remove partially the effects of lensing with an estimate of the lensing deflections obtained either from a suitably correlated tracer of large-scale structure or from the small-scale CMB itself [33–35].

Compared to lensing-induced B modes, B modes created due to patchy reionization are more difficult to disentangle from the primordial signal. This is because of our current lack of detailed

knowledge of how the Universe reionized. Reionization produces B -mode anisotropies due to inhomogeneous scattering of the local quadrupole CMB temperature anisotropy as well as anisotropic screening of the primary CMB polarization signal sourced at recombination. Several studies have estimated these B -mode signals [24, 26, 27, 36–40]. However, all of these studies have suffered from our ignorance of when and how reionization happened. The average Thomson scattering optical depth inferred from large-angle E -mode polarization has changed significantly over the last 15 years, with the central value of the implied redshift of reionization shifting from $z_{\text{re}} \sim 20$ [41] to $z_{\text{re}} \sim 7$ [42]. The best constraints on the end of reionization have resulted from observations of Lyman- α absorption features in the spectra of bright quasars. Constraining the earlier stages of reionization has been difficult, however, because the number of such quasars rapidly decreases at high redshifts. Additionally, the Lyman- α absorption saturates at neutral hydrogen fractions of $n_{\text{HI}}/n_{\text{H}} \sim 10^{-4}$ due to the large cross-section of the Lyman- α transition.

A further complication is that the level of reionization-induced B -mode anisotropy also depends on the morphology of the ionized regions created during reionization. Reionization is thought to occur due to the formation and eventual overlap of ionized regions around sources of hydrogen-ionizing radiation such as galaxies or quasars. The size and evolution of these ionized regions depend on the mass and brightness of these sources. However, the detailed nature of these sources remains unclear. Bright quasars are efficient sources of hydrogen-ionizing radiation, but their abundance at high redshifts is probably too low [43]. Galaxies are known to exist at redshifts as high as $z \sim 11$ [44], but it is unclear if hydrogen-ionizing photons produced by young stars within these galaxies can escape into the intergalactic medium without being absorbed by the in-situ hydrogen [e.g., 45–48]. For a given reionization history, reionization by quasars rather than galaxies can result in a larger amplitude of the induced secondary B modes due to the enhanced clustering of quasars [49]. Similar changes in the B -mode anisotropy amplitude can occur due to different relative contributions of bright and faint galaxies to reionization. Brighter galaxies typically reside in highly-clustered massive haloes, which can increase the anisotropy amplitude on certain scales.

As noted above, it has traditionally been difficult to get tight constraints on the redshift of reionization because the pre-eminent probe of the high-redshift intergalactic medium, the Lyman- α forest, saturates already when the neutral hydrogen fraction is around 10^{-4} . In recent years, however, excellent constraints on the redshift at which reionization ended have come from a somewhat unexpected direction. It has been noted that the Lyman- α forest at $z \approx 5.5$ exhibits spatial fluctuations that are significantly larger than those expected due to density inhomogeneities in a post-reionization Universe [50–54]. Recently, it was shown that these fluctuations are a signature of the last stages of reionization [55]. In this picture, large patches (of sizes of up to 100 comoving Mpc) of neutral hydrogen exist in low-density regions of the Universe at $z \approx 5.5$. It is these “neutral islands” that cause the observed spatial scatter in the Lyman- α forest. This interpretation yields a rather tight constraint on the redshift of the end of reionization of $z = 5.2$.

Given these developments in our understanding of reionization, providing updated estimates of the reionization-induced B -mode power is timely and of obvious interest to next-generation CMB experiments. We consider this issue in this paper.

We use hydrodynamic cosmological simulations post-processed for radiative transfer. These simulations have a large dynamic range (from around 100 comoving kpc to 160 comoving Mpc) that allows us to model the effect of small-scale reionization sources while deriving the large-scale CMB signal. They are carefully calibrated to reproduce the Lyman- α forest data, including the spatial fluctuations in the Lyman- α forest opacity. In the process, these simulations also yield a value of the Thomson scattering optical depth to the CMB last-scattering surface that is in agreement with the latest measurements reported by Planck 2018 [42]. We extrapolate these simulations to even larger length scales (1 Gpc) by using the excursion set method of modelling ionized regions in the epoch of reionization (EoR)[56]. After presenting predictions for the B -mode signal in our fiducial reionization model, we also consider the effect on this signal of the uncertainty in the first half of the reionization history and the uncertainty regarding the masses of the reionizing sources. Finally, we consider the range of values of the tensor-to-scalar ratio r that can be reliably probed by various upcoming CMB experiments in the presence of the secondary B modes from reionization.

Throughout this work we assume a flat Λ CDM universe with baryon and matter density parameters $\Omega_b = 0.0482$ and $\Omega_m = 0.308$, Hubble constant $100h \text{ km s}^{-1} \text{ Mpc}^{-1}$ with $h = 0.678$, spectral index of primordial curvature perturbations $n_s = 0.961$, clustering amplitude $\sigma_8 = 0.829$ at $z = 0$, and helium mass fraction $Y_{\text{He}} = 0.24$ [57]. The units ‘ckpc’ and ‘cMpc’ refer to comoving kpc and comoving Mpc, respectively.

2 Secondary B -mode anisotropies from reionization

After CMB decoupling at $z \sim 1100$, hydrogen and helium are essentially completely recombined and the gas in the Universe is neutral. Eventually, the first bound objects are expected to appear in the form of proto-stars around $z \sim 50$ [58]. By around $z = 5$, the ionizing radiation from galaxies and quasars reionizes the Universe [42, 55, 59]. Inhomogeneities in the distribution of matter and ionizing sources mean that different parts of the Universe will reionize at different moments in time. One consequence of this patchy reionization is that the Thomson optical depth τ , as measured to the CMB last-scattering surface, is a function of position on the sky, i.e., $\tau(\hat{\mathbf{n}})$. Patchy reionization produces secondary anisotropies in the polarization of the CMB through two mechanisms [e.g., 25, 27]: (i) polarization is generated through Thomson scattering of the local CMB temperature quadrupole anisotropy off the inhomogeneously-distributed free electrons during reionization; and (ii) the primary polarization generated by scattering around recombination is screened (i.e., polarized radiation is scattered out of the line of sight) by the anisotropic optical depth $\tau(\hat{\mathbf{n}})$. While both effects are present even in the absence of fluctuations in the free electron density, B modes will not be generated unless there are inhomogeneities. Patchy reionization will thus produce a unique signal in the B -mode polarization pattern of the CMB.

The free-electron number density during reionization varies due to inhomogeneities in the gas density and the ionization fraction, x_e . Previous semi-analytic work showed that for most plausible models, the power is dominated by the ionization rather than density inhomogeneities [60]. The ionization fraction is defined as $x_e = n_e/n_p$, i.e., the ratio of the number densities of free electrons to hydrogen nuclei. We decompose this into an average fraction \bar{x}_e and a fluctuation Δx_e , so that at comoving distance χ along a line of sight $\hat{\mathbf{n}}$ we have

$$x_e(\hat{\mathbf{n}}, \chi) = \bar{x}_e(\chi) + \Delta x_e(\hat{\mathbf{n}}, \chi), \quad (2.1)$$

where $\bar{x}_e(\chi)$ is the mean fraction at (comoving) lookback time χ and $\Delta x_e(\hat{\mathbf{n}}, \chi)$ is the fluctuation at position $\hat{\mathbf{n}}\chi$ relative to the observer at lookback time χ . The optical depth measures the line-of-sight integral of the electron density, and therefore also becomes a direction-dependent quantity on the sky. The optical depth back to lookback time χ is approximately

$$\tau(\hat{\mathbf{n}}, \chi) = \sigma_T \bar{n}_{p,0} \int_0^\chi \frac{d\chi'}{a^2} [\bar{x}_e(\chi') + \Delta x_e(\hat{\mathbf{n}}, \chi')], \quad (2.2)$$

where $\sigma_T = 6.652 \times 10^{-29} \text{ m}^2$ is the Thomson scattering cross section, $\bar{n}_{p,0}$ is the present unperturbed number density of protons and a is the scale factor. In the Limber approximation (valid for angular multipoles $\ell \gtrsim 20$) [61–63], the angular power spectrum of the optical depth fluctuations back to CMB decoupling at χ_* is

$$C_\ell^{\tau\tau} = \sigma_T^2 \bar{n}_{p,0}^2 \int_0^{\chi_*} \frac{d\chi}{a^4 \chi^2} P_{x_e x_e} \left(k = \frac{\ell}{\chi}; \chi \right). \quad (2.3)$$

Here, $P_{x_e x_e}(k; \chi)$ is the dimensional 3D power spectrum of Δx_e at lookback time χ , which satisfies $\langle \Delta x_e(\mathbf{k}, \chi) \Delta x_e(\mathbf{k}', \chi) \rangle = (2\pi)^3 \delta^{(3)}(\mathbf{k} + \mathbf{k}') P_{x_e x_e}(k; \chi)$. All the relevant astrophysical aspects of reionization are encoded in $P_{x_e x_e}(k)$. We note that $C_\ell^{\tau\tau}$ is not directly observable, although it can be reconstructed from the non-Gaussianity that patchy screening imprints in the small-scale CMB fluctuations [26, 39, 64] in a similar manner to how the CMB lensing power spectrum is reconstructed.

2.1 B -mode signal due to scattering of the CMB temperature quadrupole

To calculate the B -mode signal from reionization we need to account for the scattering probability of photons, fluctuations in the free electron density along the line of sight, and the statistics of the quadrupole moment of the temperature anisotropies through reionization. As the quadrupole of the primary temperature anisotropies, sourced around recombination, has a much larger correlation length than the fluctuations in the electron density, the B -mode power induced by scattering of the primary quadrupole simplifies, in the Limber approximation, to [25]

$$C_\ell^{BB(\text{sca})} = \frac{3}{100} \int \frac{d\chi}{\chi^2} \left[\frac{g(\chi)}{\bar{x}_e(\chi)} \right]^2 Q_{\text{rms}}^2(\chi) P_{x_e x_e} \left(k = \frac{\ell}{\chi}; \chi \right). \quad (2.4)$$

Here $g(\chi)$ is the (unperturbed) visibility function, the probability density for a photon to scatter at lookback time χ , which can be written as

$$g(\chi) = \frac{d\bar{\tau}}{d\chi} e^{-\bar{\tau}(\chi)} = \frac{\sigma_T \bar{n}_{p,0}}{a^2} \bar{x}_e(\chi) e^{-\bar{\tau}(\chi)}. \quad (2.5)$$

The quantity $Q_{\text{rms}}(\chi)$ is the r.m.s. of the primary quadrupole at lookback time χ . Given the near scale-invariance of the power spectrum of the primordial fluctuations, Q_{rms} is almost independent of χ through reionization. We take $Q_{\text{rms}} = 17 \mu\text{K}$ (e.g., [25, 26]). Combining the above equations we find

$$C_\ell^{BB(\text{sca})} = \frac{3\sigma_T^2 \bar{n}_{p,0}^2}{100} \int_{\chi_s}^{\chi_e} \frac{d\chi}{a^4 \chi^2} Q_{\text{rms}}^2(\chi) P_{x_e x_e} \left(k = \frac{\ell}{\chi}; \chi \right) e^{-2\bar{\tau}(\chi)}, \quad (2.6)$$

where χ_s and χ_e are the comoving distances to the start and end of reionization, respectively. Note the similarity to the optical depth power spectrum, Eq. (2.3), showing that the shape of the two spectra are very similar.

In the electron rest-frame, there is a further contribution to the temperature quadrupole anisotropy that is second order in the baryon peculiar velocity (the kinematic quadrupole). B -mode polarization is produced by scattering this quadrupole even in the absence of further modulation by the electron number density fluctuations [25]. We do not consider this source further in this paper since the modulated signal from patchy reionization is smaller than that from scattering the primordial quadrupole by a factor of $\bar{T}_{\text{CMB}}^2 v_{\text{rms}}^4 / Q_{\text{rms}}^2$, where $v_{\text{rms}} \sim 10^{-3} / \sqrt{1+z}$ at the relevant redshifts and \bar{T}_{CMB} is the present-day CMB temperature. Furthermore, the kinematic quadrupole has a distinct frequency dependence (e.g., Ref. [65]) that would allow removal of this source of B modes with multi-frequency data.

2.2 B -mode signal due to patchy screening

Free electrons during the epoch of reionization act as a semi-opaque screen between us and the CMB last-scattering surface. The primary anisotropies in the CMB are screened by an overall factor of $e^{-\tau(\hat{n}, \chi_*)}$ as

$$T(\hat{n}) = e^{-\tau(\hat{n}, \chi_*)} T_p(\hat{n}), \quad (2.7)$$

$$(Q \pm iU)(\hat{n}) = e^{-\tau(\hat{n}, \chi_*)} (Q \pm iU)_p(\hat{n}), \quad (2.8)$$

where T_p and $(Q \pm iU)_p$ are the primary (denoted by the superscript p) fluctuations in temperature and polarization, respectively, which would be observed in the absence of reionization. Variations in the optical depth due to the patchiness of reionization convert some of the primary E -mode into B -mode polarization. Linearising in the optical depth fluctuations, the power spectrum of these B modes is [27]

$$C_\ell^{BB(\text{scr})} = e^{-2\bar{\tau}} \int \frac{d^2 \ell_1}{(2\pi)^2} C_{\ell_1}^{EE(\text{p})} C_{|\ell-\ell_1|}^{\tau\tau} \sin^2 2(\phi_{\ell_1} - \phi_\ell), \quad (2.9)$$

where $C_{\ell_1}^{EE(p)}$ is the primary E -mode power spectrum and ϕ_{ℓ_1} is the angle between ℓ_1 and the x -direction (which corresponds to $Q > 0$).

The E -mode power peaks on small scales (around $\ell = 1000$), so large-scale B modes from patchy screening are mostly sourced by modulation of these small-scale E -modes by small-scale fluctuations in the optical depth. The resulting screened signal behaves like white noise on large scales, with a constant power spectrum given by taking the limit $\ell_1 \gg \ell$ in the integrand of Eq. (2.9) [27]:

$$C_{\ell}^{BB(\text{scr})} \approx e^{-2\bar{\tau}} \frac{1}{2} \int \frac{d^2\ell_1}{(2\pi)^2} C_{\ell_1}^{EE(p)} C_{\ell_1}^{\tau\tau}. \quad (2.10)$$

The total B -mode power spectrum induced by patchy reionization is given by the sum of the quadrupole scattering and screening spectra:

$$C_{\ell}^{BB(\text{tot})} = C_{\ell}^{BB(\text{sca})} + C_{\ell}^{BB(\text{scr})}. \quad (2.11)$$

3 Reionization model calibrated to Lyman- α forest data

As a realistic model for the inhomogeneous distribution of free electrons during the epoch of reionization, we consider the post-processed cosmological radiation hydrodynamical simulation presented by Kulkarni et al. [55] as our fiducial reionization model. The underlying cosmological hydrodynamical simulation is very similar in set-up to several simulations from the Sherwood Simulation Suite [66]. This simulation was performed using the P-GADGET-3 code, which is derived from the GADGET-2 code [67, 68]. The box size used is $L = 160h^{-1}$ cMpc. The dark matter and gas distributions are represented by 2048^3 particles each. The resultant dark matter particle mass is $M_{\text{dm}} = 3.44 \times 10^7 h^{-1} M_{\odot}$ while the gas particle mass is $M_{\text{gas}} = 6.38 \times 10^6 h^{-1} M_{\odot}$. Periodic boundary conditions are imposed and the initial conditions are set at $z = 99$. These are identical to the initial conditions of the 160–2048 simulation from the Sherwood simulation suite [66]. These initial conditions are evolved down to $z = 4$. Snapshots of the gas density and other quantities are saved at 40 Myr intervals, which results in 38 snapshots. We simplify galaxy formation in this simulation by using the QUICK_LYALPHA option in P-GADGET-3 to speed up the simulation. This removes gas particles with temperature less than 10^5 K and overdensities greater than 1000 from the hydrodynamical calculation by converting them to star particles [69]. This approximation does not affect the reionization process as the mean free path of ionizing photons is determined by self-shielded regions with a typical overdensity of $\Delta = 10$ –100 [70, 71]. Before post-processing the results of the hydrodynamic simulation, heat is injected in the gas distribution in the simulation box assuming instantaneous reionization at redshift $z = 15$ and ionization equilibrium with the metagalactic UV background modelled according to Haardt and Madau [72], marginally modified to result in inter-galactic medium (IGM) temperatures that agree with measurements [73]. Note that we do not use the ionization and temperature values that result out of this procedure; these values are instead provided by the radiative transfer calculation that is performed subsequently. The on-the-fly assumption of instantaneous reionization is made simply to ensure that the gas distribution at lower redshift has a realistic pressure smoothing, which plays a role while calibrating the simulation to Lyman- α data. An ideal approach would be to perform the radiative transfer itself on the fly, but this is still prohibitively expensive for the large dynamical ranges that we seek here. Fortunately, the absence of coupling between the radiative transfer and the hydrodynamic response to reionization heating is unlikely to affect the calibration of the simulation to the Lyman- α forest data [74] as the pressure smoothing scale at redshifts $z > 5$ for our chosen UV background is less than $100h^{-1}$ ckpc [75, 76], approximately equal to the cell size of our grid (described below). The hydrogen ionization solver assumes radiative cooling via two-body processes such as collisional excitation of H I, He I, and He II, collisional ionization of H I, He I, and He II, recombination, and Bremsstrahlung [77], and inverse Compton cooling off the CMB [78]. Metal enrichment and its effect on cooling rates is ignored.

We post-process the simulation with the radiative transfer code ATON [79, 80]. In this approach, sources of ionizing radiation are assumed to be present at the location of dark matter haloes in the simulation. We identify dark matter haloes in the output snapshots using the friends-of-friends

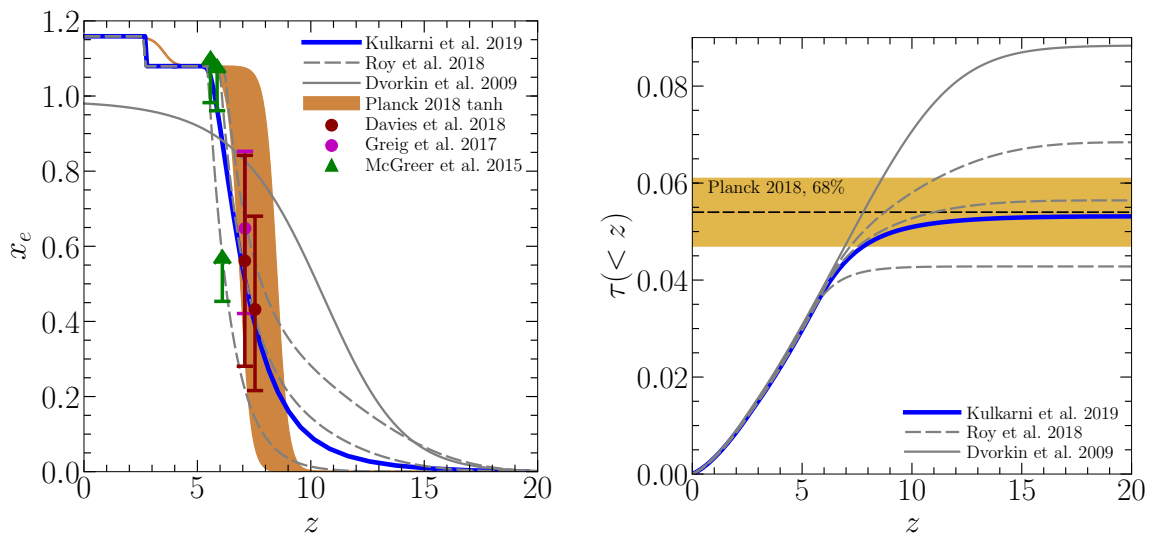


Figure 1: *Left:* Evolution of the free-electron fraction in the radiative transfer simulations of Kulkarni et al. [55] that we consider as our fiducial reionization model in this work (blue lines). Also shown are constraints from the spectra of two highest-redshift quasars [82, 83] and from the incidence of dark pixels in Ly α and Ly β forests [84]. Grey curves show reionization histories considered in earlier work [26, 39, 85] for comparison. The brown shaded region shows the 68% confidence region of the tanh reionization model reported by Planck [42]. *Right:* Cumulative electron scattering optical depth in the reionization models considered in the left panel, compared with the constraint from Planck of $\tau = 0.054 \pm 0.007$ (68% confidence) [42].

algorithm. At $z = 7$, the minimum halo mass in our simulation is $2.3 \times 10^8 h^{-1} M_\odot$, which is close to the atomic hydrogen cooling limit. The maximum halo mass at this redshift is $3.1 \times 10^{12} h^{-1} M_\odot$. We assume that a halo with mass M emits hydrogen-ionizing photons at a rate $\dot{N} = \alpha M$, where α is a free parameter that encodes our ignorance of the complex astrophysical processes, such as star formation and interaction with the inter-stellar medium, which govern the production of ionizing photons from galaxies. Note that the average ionizing photon emissivity of the simulated volume is then $\dot{n} = \alpha \sum M/V_{\text{box}}$ where $V_{\text{box}} = L^3$ is the volume of the simulation box and the summation is over all haloes. The parameter α is a function of redshift but is independent of halo mass. It is the only parameter that is varied in order to calibrate the simulation to given observations, such as the Lyman- α forest [55]. While performing the radiative transfer, we place sources only in haloes with masses greater than $10^9 M_\odot$ as the simulated halo mass function below this mass suffers from incompleteness due to lack of resolution. Further, as ATON solves the radiative transfer equation on a Cartesian grid, we project the smooth particle hydrodynamic (SPH) kernels of the gas particles in our simulation onto such a grid. We choose the number of grid cells equal to the number of gas particles in the simulation, which yields a grid resolution of $78.125 h^{-1} \text{ckpc}$. The ATON code uses a moment-based description with the M1 approximation [79] for the Eddington tensor to solve the radiative transfer equation. In order to reduce computational cost, we use a single photon frequency for the radiative transfer. We assume that all sources have a blackbody spectrum with $T = 70\,000 \text{K}$ [81]. This corresponds to an average photon energy of 23.83 eV in the optically-thick limit. The reionization history and the calibration with the Lyman- α forest are both robust to variations in the assumptions regarding the source spectrum and photon frequency. A change in the source spectrum has the effect of changing the resultant temperature of the gas distribution in the simulation. However, any resultant deviations in the Lyman- α forest can be compensated by changing α in the source emissivity above.

The calibration of our simulation with Lyman- α data is demonstrated and discussed in Ref. [55].

Here we discuss the reionization history implied by this model. The left panel of Figure 1 shows the evolution of the volume-averaged free electron fraction $x_e = n_e/n_p$ in our simulation compared with other models and data. In our model, hydrogen reionization completes rather late, at $z = 5.2$. The universe is half ionized at $z_{\text{re}} = 7$. We can quantify the duration of reionization Δz as the difference between the redshifts at which the universe is 5% and 95% reionized. In our model, we have $\Delta z = 5.4$. As Figure 1 shows, this reionization history is more gradual than the tanh models considered in the Planck 2018 results [42]. While reionization in our simulations begins earlier compared to the best-fit tanh models from Planck 2018, reionization also ends somewhat later. This reionization history is consistent with recent constraints from the spectra of two highest-redshift quasars [82, 83] and the relatively model-independent constraints from the incidence of dark pixels in Ly α and Ly β forests [84]. Note that as shown in Figure 1, we assume an instantaneous reionization of He II at $z = 2.7$ [86, 87]. We have taken into account the electrons generated during the first reionization of helium, which adds a further 8% of electrons beyond those from hydrogen reionization. The right panel of Figure 1 shows the average cumulative Thomson scattering optical depth out to $z = 20$ in our simulation. It is found to agree very well with the measurement reported by Planck 2018 [42] of $\tau = 0.054 \pm 0.007$ (68% confidence).

In Figure 1, we also show the reionization histories adopted in previous work by some of the current authors [39]. These are derived (see Section 2 of their paper for details) by solving the standard ionization/recombination balance equation for the spatially-averaged ionization fraction, and exploits the cosmic star-formation rate density by [85] based on the most recent determination of the dust-corrected UV, far-IR, and radio luminosity functions out to high redshift. In Figure 1 (left panel) we plot the reionization histories corresponding to a conservative value $f_{\text{esc}} = 10\%$ of the escape fraction of ionizing photons from primeval galaxies, and to three different values $M_{\text{UV}} = -17, -13, \text{ and } -12$ for the faintest UV magnitudes contributing to the ionizing background. The reionization history and cumulative optical depth for $M_{\text{UV}} \approx -13$ is close to that of our fiducial radiative transfer simulation. The key difference between these models and our simulation results is that the spatial distribution of the free electrons should be more realistic in the latter (which follows radiative transfer). This is important for the derived ionization power spectra and the induced B -mode power spectra, which we discuss below.

The box size L determines the largest scale accessible in our reionization model. This corresponds to the fundamental mode of the box, which is given by $k_f = 2\pi/L$. For the fiducial simulation described above the box size is $L = 160h^{-1} \text{ cMpc}$, which implies $k_f = 0.039h \text{ cMpc}^{-1}$. The value of k_f determines the minimum multipole, ℓ_{min} , we can calculate the angular power spectra at as we have $\ell \approx k_f \chi(z)$. This allows us to reach down to $\ell_{\text{min}} \approx 430$ in the $L = 160h^{-1} \text{ cMpc}$ radiative transfer simulations. However, the angular power spectrum of the primordial B -mode signal peaks around $\ell \sim 100$. To assess the contribution from patchy reionization on such scales, we need to extend the size of the simulation. It is computationally prohibitive to increase the box size L significantly in the radiative transfer simulations. Instead, we adopt a well-known semi-numerical method based on the excursion set approach to modelling reionization. We validate this method by matching its reionization history to that of our radiative transfer simulation and by comparing the ionization power spectra on scales where there is overlap. In this way, we use the semi-numerical method to model the free electron distribution during the epoch of reionization up to scales of 1 cGpc , which corresponds to a minimum multipole $\ell_{\text{min}} \approx 50$, below the multipole where the primordial signal is expected to peak. The simulation with $L = 1h^{-1} \text{ cGpc}$ has the same halo mass resolution as the radiative transfer simulation of reionization.

We use the 21cmFAST code [88, 89] to generate the density field from redshift $z_{\text{start}} = 19.5$ to $z_{\text{end}} = 4.97$ at 40 Myr intervals. Gaussian initial conditions are set on a 3584^3 grid at $z \approx 300$. 21cmFast then calculates the linear displacement field on a coarser 512^3 grid using the Zel'dovich approximation [90, 91]. These displacements are then used to update the particle positions in the initial density field. This method of generating large-scale density fields using the Zel'dovich approximation is computationally efficient and has been validated by several works [e.g., 89, 92–94]. The coarse resolution of the grid is sufficient for our purposes as we are primarily interested in the large-scale distribution of ionized hydrogen. Next, we identify haloes with masses above $10^9 M_\odot$ using the

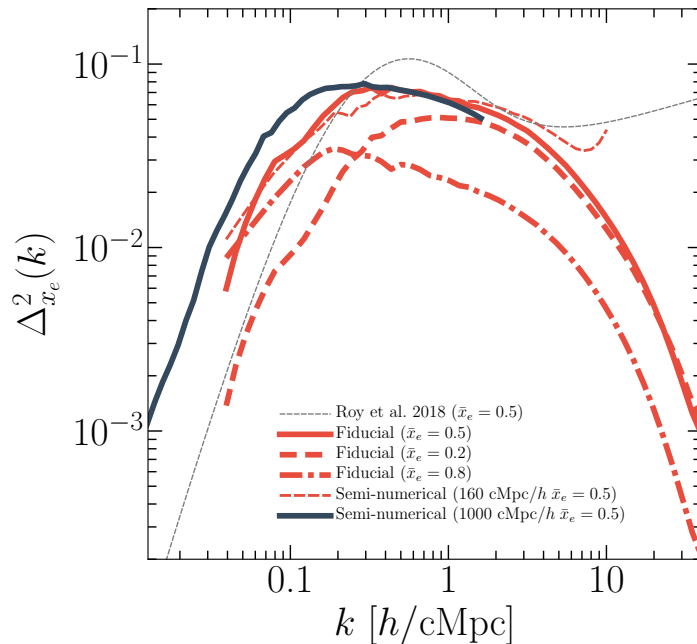


Figure 2: Dimensionless power spectra of the ionized hydrogen fraction from our fiducial radiative transfer simulation (thick red curves) at redshifts corresponding to average ionization fractions of $\bar{x}_e = 0.8$ (dot-dashed), 0.5 (solid) and 0.2 (dashed). The thin-dashed red curve shows the same for $\bar{x}_e = 0.5$ from the semi-numerical method implemented in a $L = 160h^{-1}$ cMpc long box and the thick black curve for $L = 1 h^{-1}$ cGpc. The power spectrum at $\bar{x}_e = 0.5$ from a semi-analytic method used in recent work by some of the authors [39] is shown for comparison (thin grey dashed).

extended Press–Schechter formalism [95, 96]. 21cmFAST finds haloes iteratively by smoothing the density field at progressively smaller scales and identifying haloes of a given mass as regions where the smoothed overdensity in the (Zel’dovich-evolved) field first exceeds that for gravitational collapse, $\delta_c = 1.686$. A real space top-hat filter is used for smoothing the density field and assigning masses to the haloes.

Given the density field and haloes, we derive the ionization field by placing sources of Lyman-continuum radiation in dark matter haloes and using the excursion-set method [97–99]. Similar to our radiative transfer simulation above, the total number of ionizing photons N_γ produced by a halo is assumed to be proportional to the halo mass [100]:

$$N_\gamma(M) = N_\gamma^{\text{LyC}} M / m_p, \quad (3.1)$$

where the dimensionless proportionality factor N_γ^{LyC} includes the Lyman-continuum escape fraction and m_p is the proton mass. A grid cell at position \mathbf{x} is ionized if the condition

$$\langle n_\gamma(\mathbf{x}) \rangle_R > \langle n_p(\mathbf{x}) \rangle_R (1 + \bar{N}_{\text{rec}}), \quad (3.2)$$

is satisfied in a spherical region centred on the cell for some radius R [98, 99, 101]. Here, the averages are over the spherical region, n_p is the number density of hydrogen nuclei,

$$n_\gamma = \int_{M_{\text{min}}}^{\infty} dM \left. \frac{dN}{dM} \right|_R N_\gamma(M), \quad (3.3)$$

where $dN/dM|_R$ is the halo mass function within the spherical region, M_{min} is the minimum halo mass that contributes ionizing photons, and \bar{N}_{rec} is the average number of recombinations per hydrogen

atom in the IGM. (We note that the global volume average of n_p is \bar{n}_p .) The condition in Eq. (3.2) simply requires that a sufficient number of photons have been produced in a spherical region of radius R to have ionized all the hydrogen atoms in that region, and to have maintained this ionization state in the presence of \bar{N}_{rec} recombinations per atom. It can be recast as

$$\zeta_{\text{eff}} f(\mathbf{x}, R) \geq 1, \quad (3.4)$$

where the quantity

$$f = \rho_m(R)^{-1} \int_{M_{\text{min}}}^{\infty} dM \left. \frac{dN}{dM} \right|_R M, \quad (3.5)$$

is the collapsed fraction into haloes of mass $M > M_{\text{min}}$ within the spherical region centred on \mathbf{x} , M_{min} is the minimum mass of halos that emit Lyman continuum photons, and $\rho_m(R)$ is the average matter density within the sphere. The parameter ζ_{eff} quantifies the number of photons in the IGM per hydrogen atom in stars, accounting for hydrogen recombinations in the IGM. We can write ζ_{eff} in terms of the parameters of Eqs (3.1) and (3.2) as

$$\zeta_{\text{eff}} = \frac{N_{\gamma}^{\text{LyC}}}{1 - Y_{\text{He}}} (1 + \bar{N}_{\text{rec}})^{-1}, \quad (3.6)$$

where Y_{He} is the helium mass fraction. The parameter ζ_{eff} is the only parameter that determines the ionization field in this approach. The volume-weighted ionized fraction in the simulation box is $Q_V \equiv \sum_i Q_i / n_{\text{cell}}$, where the ionized volume fraction in a cell i is Q_i and n_{cell} is the total number of grid cells. We tune ζ_{eff} to ensure that our 1 cGpc box has the same reionization history as the radiative transfer simulation described above.

We derive the 3D power spectrum of the electron fraction by averaging $|\Delta x_e(\mathbf{k})|^2$, where $\Delta x_e(\mathbf{k})$ is the Fourier transform of the free electron fraction, within a spherical shell of radius k . Figure 2 shows the dimensionless power spectrum $\Delta_{x_e}^2(k) = k^3 P_{x_e x_e}(k) / (2\pi^2)$ at three different redshifts in our fiducial radiative transfer simulation. The power spectrum peaks when the global ionization fraction is close to 50%, before this time there are few free electrons and later the IGM is fully ionized so the electron fraction is smooth. In the same figure we also compare the power spectrum from our fiducial simulation with an implementation of the semi-numerical scheme in a box of the same size ($L = 160h^{-1}$ cMpc on a side). This semi-numerical implementation is tuned to have an identical reionization history as our fiducial radiative transfer simulation by choosing an appropriate value for the ζ_{eff} parameter as described above. We find that the power spectrum of the electron fraction from the semi-numerical approach agrees very well with that from the radiative transfer simulation. The difference in power is less than 10% on most scales. This validates the semi-numerical approach and our calibration of it. To extend beyond the lowest wavenumber k that we can probe, we proceed to consider the semi-numerical scheme in larger boxes with $L = 500h^{-1}$ cMpc (not shown in Figure 2) and $L = 1000h^{-1}$ cMpc. These larger simulations are also tuned to have the same reionization history as the fiducial radiative transfer simulation. They have very similar power as the fiducial simulation on small scales but additional power on large scales (see Figure 2)¹. This additional power arises from ionized regions around rare, high-mass haloes that are not present in the smaller box. The agreement on small scales is good because we use the same minimum halo mass value of $10^9 M_{\odot}$ in every semi-numerical simulation. For comparison with earlier work, we include in Figure 2 the power spectrum at $\bar{x}_e = 0.5$ from a semi-analytical model of reionization used in Ref. [39]. One-bubble correlations dominate on scales $k \geq 1$ cMpc⁻¹ while large scales are dominated by the correlation between different ionized bubbles.

4 Results

4.1 Power spectrum of secondary B -mode anisotropies

In this section we estimate the B -mode signal from patchy reionization and calculate its contamination in the search for the primordial signal. Figure 3 (left panel) compares the angular power spectrum of

¹As we use a fixed number of grid points, we cannot measure the power spectrum in the large box to such small scales as in the fiducial simulations.

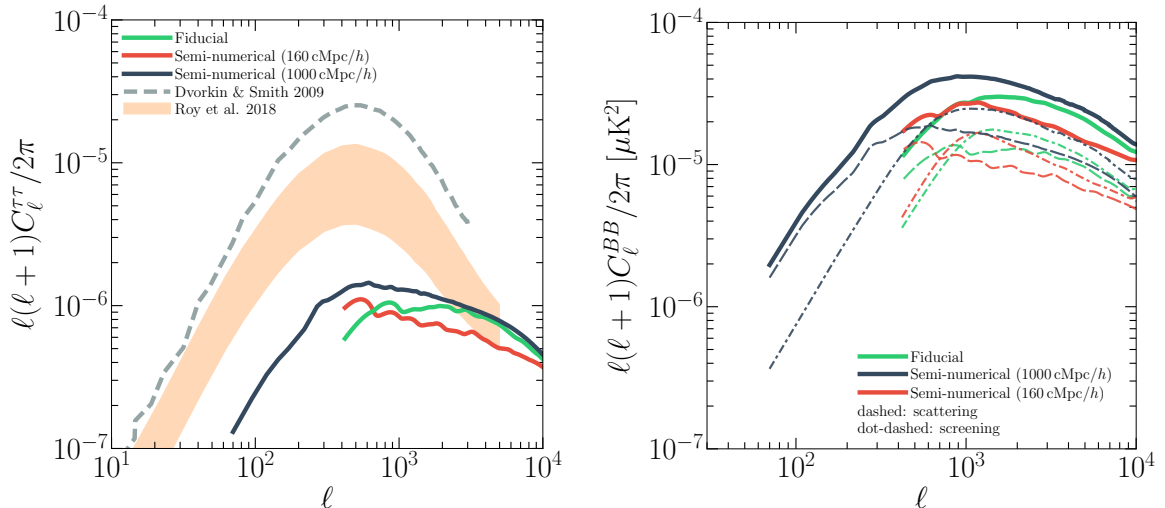


Figure 3: *Left:* The angular power spectrum of the Thomson scattering optical depth in our fiducial radiative transfer simulation (green curve), semi-numerical simulation in the $160h^{-1}$ cMpc box (red curve), and the semi-numerical simulation in the $1h^{-1}$ cGpc box (black curve). All three simulations have the same reionization histories. The dashed grey curve in this panel shows the power spectrum from [26] for comparison. The shaded region corresponds to the range of power spectra derived previously [39]. *Right:* B -mode power spectrum from patchy reionization, with the same color coding as the left panel. The dashed and dot-dashed curves show the quadrupole scattering and screening contributions, respectively, to the power spectrum and the solid lines are their total.

the Thomson optical depth fluctuations from the fiducial radiative transfer simulation to those from the semi-numerical simulations using the excursion set algorithm (calibrated to the radiative transfer simulation, as described in Section 3). The optical depth power spectrum $C_\ell^{\tau\tau}$ agrees reasonably well at multipoles $\ell \gtrsim 700$ for the various simulations. (Some level of disagreement is expected as the radiative transfer is much better at computing the ionization field around the edges of the bubble [102].) The figure also compares our simulation results to earlier work by other authors [26]. The power spectrum $C_\ell^{\tau\tau}$ from the $1h^{-1}$ cGpc box is roughly 20 and 15 times smaller than the fiducial model studied by [26] at $\ell \approx 100$ and $\ell \approx 1000$, respectively. The same toy model of reionization is used by Refs. [26] and [39] but their reionization histories are different. The optical depth used in [26] is higher than [39], hence $C_\ell^{\tau\tau}$ is larger.

The right-hand panel of Figure 3 shows the B -mode angular power spectrum due to patchy reionization. The B modes from quadrupole scattering (dashed lines) exceed those from patchy screening (dot-dashed lines) on large scales, $\ell \lesssim 600$, across all our simulations. As noted in Section 2.2, the B modes from patchy screening are sourced by a modulation of the primary E modes and have white-noise power on scales large compared to the peak of the E -mode power spectrum ($\ell \approx 1000$). The large-scale B -mode power is determined by the small-scale fluctuations in the optical depth, where the E -mode power is significant. In contrast, large-angle B modes due to quadrupole scattering depend on the large-scale power of $C_\ell^{\tau\tau}$. Since the latter is dominated by the shot noise of the bubbles, the B -mode power from scattering is also white on scales large compared to the typical bubble size.

The total C_ℓ^{BB} across our different simulations peaks in the range $\ell = 1000$ – 2000 (in the remainder of this paper, C_ℓ^{BB} will always refer to this total B -mode signal from patchy reionization, i.e., the sum of scattering and screening contributions). The shape of the angular power spectrum due to scattering closely follows $C_\ell^{\tau\tau}$ (see Eq. 2.6). It peaks on larger scales than the screening contribution, as the latter turns over near the peak of the primary E -mode spectrum. The maximum amplitude of the total C_ℓ^{BB} derived from the semi-numerical method for the $L = 1h^{-1}$ cGpc box is around twice that of

our fiducial radiative-transfer simulation. This is due to the presence of large bubbles around massive haloes that are present in the $L = 1h^{-1}$ cGpc box but are absent in the smaller $L = 160h^{-1}$ cMpc box.

In Figure 4 we compare the B -mode angular power spectrum from patchy reionization to the primordial B -mode power from gravitational waves and the instrumental noise power spectra expected for forthcoming and proposed experiments. The noise spectra are modelled as $N_\ell^{BB} = \Delta_P^2 \exp[\ell(\ell+1)\Theta_f^2/(8\ln 2)]$ [103]. Here, Δ_P is the polarization noise level in the maps and Θ_f is the full-width half-maximum (FWHM) of the beam. We consider four experimental configurations; two ground-based and two satellite missions. For the ground-based experiments we consider $\Delta_P = 3.0 \mu\text{K-arcmin}$ and $\Theta_f = 17 \text{ arcmin}$, corresponding to the goal white-noise level at 145 GHz for the Simons Observatory small-aperture telescope (SAT) survey [104], and $\Delta_P = 1.5 \mu\text{K-arcmin}$ and $\Theta_f = 30 \text{ arcmin}$, corresponding roughly to the planned SAT survey from CMB-S4 [15, 105]. The combination of limited sky coverage and low-frequency atmospheric noise will limit the largest scales accessible to these ground-based surveys ($\ell \sim 30$ in polarization). For the full-sky satellite surveys, we consider $\Delta_P = 2.4 \mu\text{K-arcmin}$ and $\Theta_f = 30 \text{ arcmin}$, corresponding to the total sensitivity of the LiteBIRD satellite [106]. More sensitive satellite missions have also been proposed; here we consider PICO [107] with $\Delta_P = 0.85 \mu\text{K-arcmin}$ and $\Theta_f = 7.9 \text{ arcmin}$. Several ground-based instruments, such as AdvACT [108], SPT-3G [3], BICEP3 [109], and Simons Array [110], are operating at present but with lower sensitivity than the noise curves shown in Figure 4. Future space CMB missions will aim to measure the primordial B -mode signals from both (global) reionization at $\ell \leq 20$ and recombination, which peaks around $\ell \approx 100$, while ground-based surveys will mostly target the recombination signal. In Figure 4, we show three primordial B -mode power spectra corresponding to tensor-to-scalar ratios $r = 10^{-2}$, 10^{-3} and 10^{-4} . The current best constraint on r comes from joint analysis of B -mode data from BICEP/Keck Array, Planck and WMAP: $r < 0.06$ at 95% confidence [13].

CMB photons are also lensed due to the gravitational potential of matter along the line of sight. Primary E modes are transformed into lensed B modes, even if there is no primordial B -mode signal. On the large scales of interest, the B modes due to lensing can be considered as white noise with a corresponding $\Delta_P \approx 5 \mu\text{K-arcmin}$. Future (ground-based) CMB experiments will need to remove the lensing B -mode signal using “delensing” techniques to probe primordial gravitational waves for $r \leq 10^{-3}$. The sum of the primordial and lensing B -mode power is also shown in Figure 4 for $r = 10^{-3}$.

The B -mode power from patchy reionization shown in Figure 4 (red line) is from the semi-numerical method in the larger $L = 1h^{-1}$ cGpc box. As discussed in Section 3, this should be our most reliable estimate of the large-scale power. We compare this with the power estimated in previous studies using a semi-analytic model [26, 39, 111]. These semi-analytic studies predict a larger B -mode power than our simulations. We note that the reionization history used in Ref. [26] was based on WMAP data for which $\tau = 0.089$, partly accounting for the increased B -mode power (see Section 4.2). A further relevant factor is the larger characteristic bubble radius used in the earlier works ($R_b \approx 5 \text{ cMpc}$). Typically, the B -mode signal due to patchy reionization peaks at a scale comparable to R_b , with larger characteristic radius shifting the peak in the power spectrum to smaller angular multipoles. In our simulation-driven results, the peak power is around $\ell \sim 1000$ (close to the peak in the lensing power), whereas for the bubble radii adopted in earlier semi-analytic models the peak is in the range $\ell = 100\text{--}500$. Our estimate of the large-scale B -mode power is consistent with that in recent work [40] using photon-conserving semi-numerical simulations (dashed purple line in Fig. 4) and a reionization history consistent with the central value of the optical depth from Planck [42] ($\tau \approx 0.055$). We compare with their results for a minimum halo mass $M_{\text{min}} = 10^9 M_\odot$, consistent with the choice in our simulations. While Ref. [40] considered only the quadrupole scattering contribution, we also include screening. However, on large scales, $\ell \lesssim 100$, the B modes from scattering dominate.

It is clear from Fig. 4 that patchy reionization will have a limited impact on searches for primordial B -modes from the next generation of surveys that are targeting $r \gtrsim 10^{-3}$. However, it may become relevant for $r \lesssim 10^{-4}$. (We discuss these issues more quantitatively in Section 4.4.) Given the shape of the signal from patchy reionization, it is a negligible contaminant in searches for B modes from gravitational waves sourced by homogeneous scattering at reionization (i.e., at $\ell \lesssim 20$), targeted by

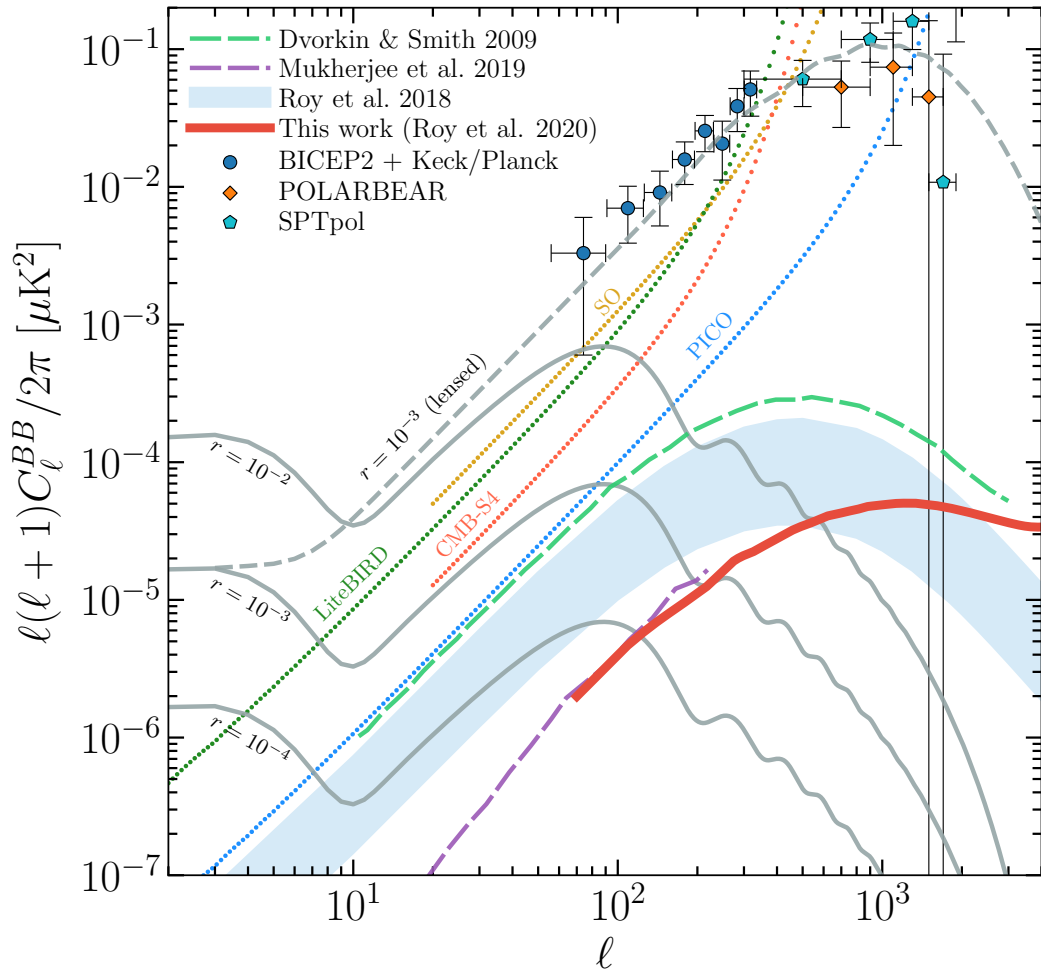


Figure 4: Comparison of the B -mode power spectrum from patchy reionization (red solid curve) for our $L = 1h^{-1}$ cGpc semi-numerical simulation with the primordial B -mode spectrum (solid grey curves) for tensor-to-scalar ratios $r = 10^{-2}$, 10^{-3} and 10^{-4} . Also shown are previous estimates of the reionization-induced signal [26, 39, 40]. Dotted curves show the instrumental noise power spectra for PICO (blue), CMB-S4 (red), LiteBIRD (green), and Simons Observatory (yellow). The sum of the primordial and lensing-induced B -mode power is shown for $r = 10^{-3}$ as the dashed grey curve. Data points show B -mode power measurements from BICEP2/Keck Array [17] (after foreground cleaning), POLARBEAR [112] and SPT [32].

future space missions such as the LiteBIRD and PICO [106, 107].

4.2 Effect of reionization history

Within our semi-numerical framework we can easily vary the reionization history to explore its impact on the B -mode power from patchy reionization. We adopt a simple tanh functional behaviour, parameterized by the mean redshift of reionization, z_{re} , and the width of the reionization, Δz . The ionization fraction evolves as

$$x_e(z) = \frac{f}{2} \left[1 + \tanh \left(\frac{y_{\text{re}} - y}{\Delta y_{\text{re}}} \right) \right], \quad (4.1)$$

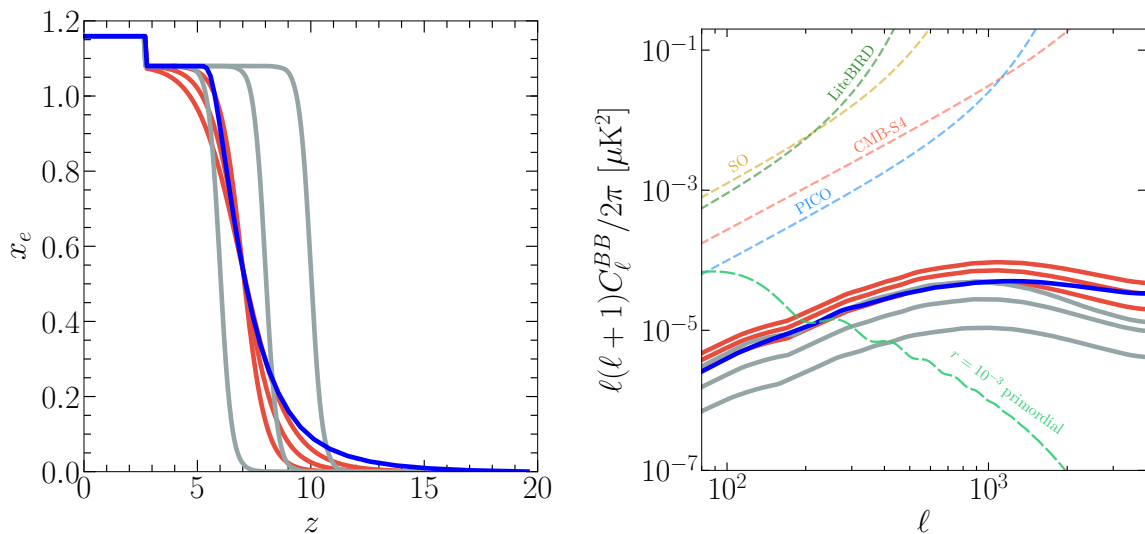


Figure 5: *Left:* Reionization histories for the tanh parameterization of Eq. (4.1) compared to our fiducial model (blue). The red curves show the effect of varying the reionization duration $\Delta z_{\text{re}} = 1, 1.5$ and 2 at fixed mean redshift $z_{\text{re}} = 7$. The grey curves instead vary $z_{\text{re}} = 6, 8$ and 10 for fixed $\Delta z_{\text{re}} = 0.5$. *Right:* Corresponding B -mode power spectra calculated with our semi-numerical method, with the same colour coding as the left panel. The amplitude of the B -mode power is higher for larger z_{re} and Δz_{re} . The dashed curves show noise power spectra for the same surveys as in Figure 4 and the primordial signal for the tensor-to-scalar ratio $r = 10^{-3}$ (green).

where $y(z) = (1+z)^{3/2}$, $y_{\text{re}} = y(z_{\text{re}})$ and $\Delta y_{\text{re}} = 1.5\sqrt{1+z_{\text{re}}}\Delta z_{\text{re}}$ [113]. Accounting for the first reionization of helium, we have $f \approx 1.08$. In the left panel of Figure 5 we show example reionization histories varying z_{re} and Δz_{re} . We note that some of these histories would be excluded by constraints on τ from Planck, but are included to illustrate more obviously the impact of the reionization history on the B -mode power from patchy reionization.

In the right panel of Figure 5 we show the B -mode power from patchy reionization computed within our semi-numerical framework for the reionization histories shown in the left panel. The amplitude of the B -mode power spectrum increases for earlier reionization and with the duration Δz_{re} . For the duration, the main effect is just that more variance is accumulated because of the increased duration of the patchy phase. For the timing, the signal increases due to the higher density if reionization happens earlier.

4.3 Minimum mass of reionization sources

In our fiducial simulation, sources of reionizing radiation are placed in haloes with masses down to $10^9 M_{\odot}$. The mass of reionization sources will have an effect on the clustering of the free electron distribution during reionization [49, 114], which can in turn change the induced secondary B modes. The agreement of our radiative transfer simulation with a variety of data [55, 115] suggests that sources in haloes down to $10^9 M_{\odot}$ should be able to reionize the universe. Still, the mass of reionizing sources is unfortunately unknown. The fraction of hydrogen-ionizing radiation produced in a galaxy that can escape into the intergalactic medium and cause reionization is largely uncertain. This escape fraction has been measured in a handful of relatively bright and low-redshift galaxies [46, 47, 116, 117, 117–126] but is unknown for the galaxies within the epoch of reionization. The escape fraction can be a function of halo mass and can influence, e.g., the relative contribution of highly-clustered massive haloes and low-mass haloes to reionization. Furthermore, active galactic nuclei (AGN), which are known to have unit escape fraction, can also reionize the universe instead of star-forming galaxies.

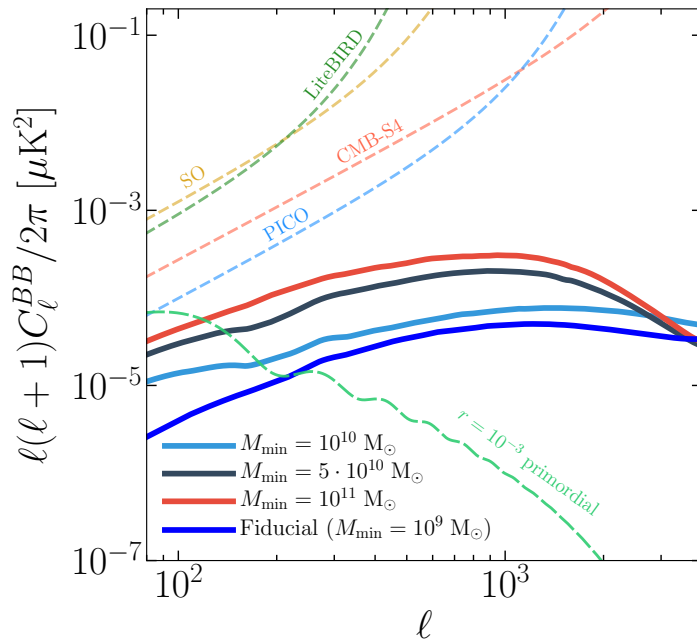


Figure 6: Dependence of the induced B -mode power spectrum on the minimum mass of reionizing sources for a fixed reionization history. Sources in higher-mass haloes induce larger B -mode power due to their stronger clustering. The dashed curves show noise power spectra for the same surveys as in Figure 4 and the primordial signal for the tensor-to-scalar ratio $r = 10^{-3}$ (green).

Such a scenario, although unlikely [43], can potentially have a large effect on the induced B -mode signal as AGN reside in very high mass haloes that are highly clustered [49].

In Figure 6, we increase the minimum mass of reionizing sources in our model from $M_{\min} = 10^9 M_\odot$ to $10^{11} M_\odot$. This is done using the excursion-set-based treatment described in Section 3. The reionization history is always kept the same as our fiducial simulation (Figure 1) by changing the brightness of each halo suitably, i.e., by tuning the parameter N_γ^{LyC} in Eq. (3.1). As a result, as M_{\min} is increased the ionized regions increase in size and become more clustered [49]. This results in an enhancement of about an order of magnitude in the induced B -mode power spectrum, as seen in Figure 6.

4.4 Constraints on the tensor-to-scalar ratio

We now quantitatively consider the effect of reionization-induced secondary B modes on the inference of the tensor-to-scalar ratio from the B -mode power spectrum.

The primordial B -mode power spectrum peaks around $\ell \approx 100$, where the signal is generated by scattering at recombination. Current and future CMB polarization experiments aim to target this recombination peak in the search for primordial gravitational waves. For small values of the tensor-to-scalar ratio r , the signal-to-noise ratio (S/N) is expected to be less than one per mode (see Figure 4), but such small signals can still be detected if the information across multiple modes is combined [7, 15, 104, 127]. Also, foreground contamination due to emission from the Galaxy exceeds the primordial signal at the recombination peak in even the cleanest regions of the sky for $r = 10^{-2}$ [17, 103, 128, 129]. As a result, the precise shape of the B -mode power spectrum will be hard to determine for small r and it will be a challenge to distinguish the primordial signal from secondary B modes induced by other sources if the shape of the secondary B -mode power spectrum is not sufficiently dissimilar within the range of multipoles considered.

Let us begin by assuming that no attempt is made to account for the additional B -mode power from patchy reionization when constraining r . Generally, we can calculate the bias introduced by

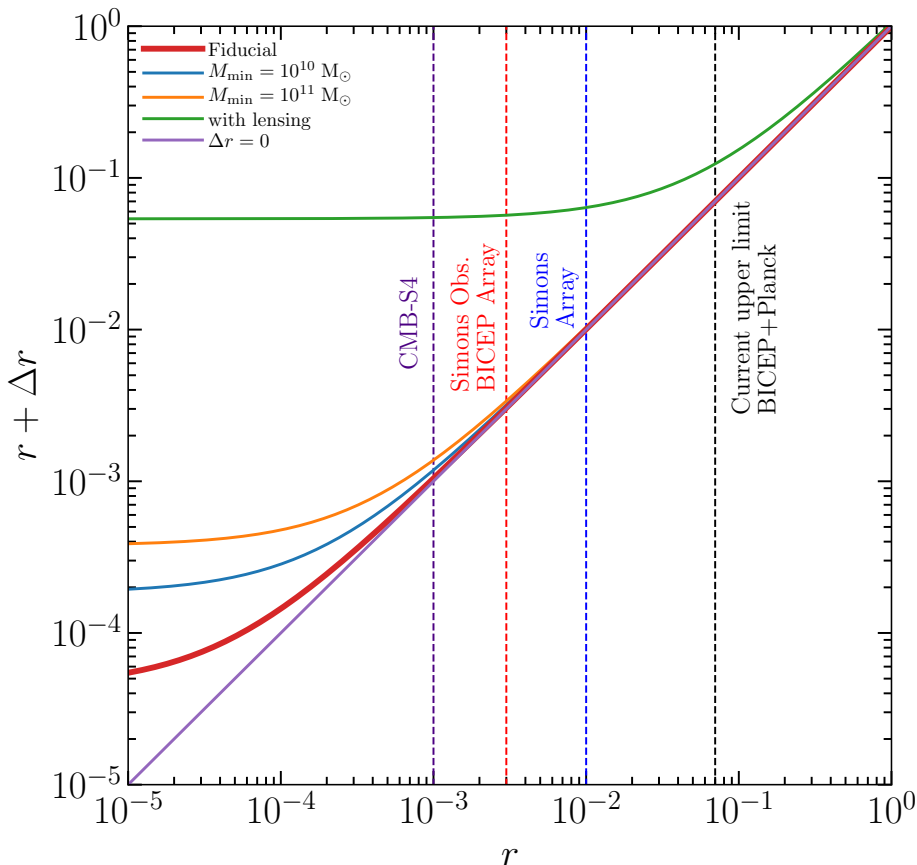


Figure 7: Bias on the tensor-to-scalar ratio inferred from the B -mode power spectrum in the multipole range $70 \leq \ell \leq 200$ when secondary sources of B -mode power are not accounted. The red curve corresponds to the case where the reionization-induced B -mode signal is the only unaccounted secondary signal. Blue and orange curves show how this bias increases with the minimum halo mass hosting ionized sources. The green curve shows the bias if the lensing is disregarded. Vertical lines show the current upper limit on r and predicted experimental sensitivities for Simons Array, BICEP Array [2], Simons Observatory [4], and CMB-S4 [5].

unaccounted-for secondary anisotropies as

$$\Delta r = \left(\sum_{\ell=\ell_{\min}}^{\ell_{\max}} [C_{\ell}^{BB}(r=1)]^2 / \Delta C_{\ell}^2 \right)^{-1} \sum_{\ell=\ell_{\min}}^{\ell_{\max}} C_{\ell}^{BB(\text{sec})} C_{\ell}^{BB}(r=1) / \Delta C_{\ell}^2. \quad (4.2)$$

Here, $C_{\ell}^{BB(\text{sec})}$ is the secondary B -mode power from non-primordial sources such as lensing, patchy reionization, and foreground emission, and $C_{\ell}^{BB}(r=1)$ is the primary power for $r=1$. The minimum and maximum multipoles used in the analysis are denoted by ℓ_{\min} and ℓ_{\max} , respectively. We focus on multipoles targeted by ground-based experiments around the peak of the primary power from recombination and assume $\ell_{\min} = 70$ and $\ell_{\max} = 200$. The variance of the total B -mode power is ΔC_{ℓ}^2 which is approximately $2C_{\ell}^2 / [(2\ell+1)f_{\text{sky}}]$, where f_{sky} is the fraction of sky in the survey.

Figure 7 shows the bias on r for our fiducial reionization model, and the effect of increasing the minimum halo mass hosting ionizing sources. Secondary B modes from patchy reionization can bias the tensor-to-scalar ratio r for $r < 10^{-3}$. At the sensitivity level of future ground-based experiments (r around 10^{-3}), reionization-induced B modes could generate a fractional bias between 10% and 30% for $M_{\min} = 10^9 M_{\odot}$ (our fiducial model) and $10^{11} M_{\odot}$, respectively. For a future satellite experiment

(e.g., PICO [7] or CMB Bharat [8]) targeting $r = 5 \times 10^{-4}$, the bias could be in the range 35–75% as M_{\min} varies from $10^9 M_{\odot}$ to $10^{11} M_{\odot}$, respectively, if these experiments used only the recombination signal. However, these space-based missions will constrain r by probing both the recombination and reionization signal. The latter will be negligibly biased by reionization for detectable levels of r .

In practice, future CMB experiments will search for the primordial B -mode signal in the presence of the lensing signal, instrumental noise and foregrounds. The lensing-induced B modes can be partly removed using high-resolution polarization measurements over an overlapping sky region along with some estimate for the lensing deflections, obtained either from the CMB itself or in combination with other correlated tracers, in a process known as delensing. The residual B -mode power after delensing, and any residual foregrounds after cleaning with multi-frequency data, will likely be dealt with by marginalising over the amplitudes of suitable template power spectra as part of the likelihood analysis used to estimate the tensor-to-scalar ratio. In such an analysis, we would model the B -mode spectrum as

$$C_{\ell}^{BB} = \sum_i \alpha_i C_{\ell}^{BB(i)}, \quad (4.3)$$

where α_i are the parameters we wish to constrain jointly, with $\alpha_1 = r$ and the other parameters are amplitude parameters for different sources of secondary power (e.g., residual lensing and patchy reionization). The template spectrum for the i th parameter is $C_{\ell}^{BB(i)}$, which reduces to $C_{\ell}^{BB}(r=1)$ for $i=1$ and to the appropriate secondary power template for $i>1$. The maximum-likelihood estimates for the parameters are

$$\hat{\alpha}_i = \sum_j (F^{-1})_{ij} \sum_{\ell=\ell_{\min}}^{\ell_{\max}} C_{\ell}^{BB(j)} \hat{C}_{\ell}^{BB} / \Delta C_{\ell}^2, \quad (4.4)$$

where \hat{C}_{ℓ}^{BB} is the measured power spectrum (with any instrument noise bias subtracted) and the Fisher matrix for the parameters is

$$F_{ij} = \sum_{\ell=\ell_{\min}}^{\ell_{\max}} C_{\ell}^{BB(i)} C_{\ell}^{BB(j)} / \Delta C_{\ell}^2. \quad (4.5)$$

After marginalising over the amplitudes of the secondary spectra, the error on the tensor-to-scalar ratio is $(F^{-1})_{11}$.

In the forecasts below, we assume polarization noise $\Delta_P = 1.5 \mu\text{K-arcmin}$ and a beam size $\Theta_f = 30 \text{ arcmin}$. We further assume that the lensing power has been reduced by 90% through delensing. We set the sky fraction to $f_{\text{sky}} = 1$, noting that statistical errors on parameters scale as $f_{\text{sky}}^{-1/2}$ while biases are independent of f_{sky} . In this experimental configuration, we find that the statistical error on r is $\sigma(r) = 1.3 \times 10^{-4}$ without marginalising over the amplitude of the patchy B -mode power from reionization. The bias on r from patchy reionization ranges from 5.5×10^{-5} to 6.3×10^{-4} as the minimum halo mass ranges from $M_{\min} = 10^9 M_{\odot}$ to $M_{\min} = 10^{11} M_{\odot}$, assuming no correction is made. If instead we marginalise over patchy reionization, with a template corresponding to our fiducial model with minimum halo mass $M_{\min} = 10^9 M_{\odot}$ (and no prior on the amplitude), we find that that $\sigma(r)$ increases to 2×10^{-4} .

The maximum-likelihood parameter estimates are unbiased if the templates have the correct shape: $\langle \hat{\alpha}_i \rangle = \alpha_i^{\text{true}}$, where α_i^{true} are the true parameter values. However, if there is some error in the I th template, so the true power in Eq. (4.3) has an additional contribution $\delta C_{\ell}^{BB(I)}$, the parameter means become

$$\langle \hat{\alpha}_i \rangle = \alpha_i^{\text{true}} + \sum_j (F^{-1})_{ij} \sum_{\ell=\ell_{\min}}^{\ell_{\max}} C_{\ell}^{BB(j)} \delta C_{\ell}^{BB(I)} / \Delta C_{\ell}^2. \quad (4.6)$$

We note that only the I th parameter mean changes if $\delta C_{\ell}^{BB(I)} \propto C_{\ell}^{BB(I)}$, corresponding to a change in amplitude of the I th source of power. However, if there is an error in the *shape* of the template, this template mismatch can bias constraints on r . We assess this level of bias by considering an extreme

case where the true model has a minimum halo mass $M_{\min} = 10^{11}M_{\odot}$, but the template assumed in the analysis has $M_{\min} = 10^9M_{\odot}$. Without marginalisation, the bias on r is 6.3×10^{-4} , as discussed above. However, with marginalisation, although with an incorrect template, the bias falls significantly to 9.9×10^{-5} , which is around half the (marginalised) full-sky statistical error on r .

We have not assumed any prior on the amplitude of the power from patchy reionization in these forecasts. Given our current theoretical uncertainties – for example, over the relevant multipole range the maximum ratio of power in the models with $M_{\min} = 10^9M_{\odot}$ and $M_{\min} = 10^{11}M_{\odot}$ is around 13 – the B -mode measurements should be sufficiently informative to differentiate between our fiducial and more extreme models for the patchy power, and so adopting a prior that brackets the theoretical uncertainty would give little improvement in the marginalised statistical error on r . In fact, adopting such a prior risks exacerbating the bias in r since both template mismatch and errors in the central value of the prior can lead to bias in this case. For reference, in our fiducial $M_{\min} = 10^9M_{\odot}$ case, the marginalised error on the amplitude of the template is $\sigma(\alpha) = 2.7$, which is insufficient to detect the power in the fiducial model ($\alpha = 1$) but would rule out the $M_{\min} = 10^{11}M_{\odot}$ model at high significance.

5 Discussion

We have investigated the imprint of patchy reionization on the cosmic microwave background B -mode polarization. The B -mode power from patchy reionization depends on the reionization history and the morphology and clustering of the ionized regions. Compared to previous studies, we used realistic radiative transfer simulations of reionization to estimate the B -mode signal. These simulations are calibrated to match the Thomson scattering optical depth measured by *Planck* and the mean transmission fraction of the Ly α forest. With this calibration, these simulations have been found to match successfully a variety of observations related to reionization, such as the observed spatial fluctuations in the Ly α opacity of the IGM, the ionization fraction inferred from the frequency of dark pixels in Ly α forest spectra, quasar near zones, as well as the Ly β opacity of the IGM. While these radiative transfer simulations model reionization on scales up to $160h^{-1}$ cMpc (i.e., 236 cMpc), we extrapolate them up to scales of 1 cGpc by using an excursion-set-based approach. In this model, reionization begins at redshift $z \approx 15$, is halfway complete at $z = 7$, and finishes at $z = 5.2$.

We find that the B -mode power at multipoles $l \approx 100$ due to scattering and screening of CMB photons during reionization (scattering dominates on these scales) is more than one order of magnitude lower than the primary B -mode from primordial gravitational waves with a tensor-to-scalar ratio $r = 10^{-3}$. The power from patchy reionization is comparable to the power of the primary signal for $r \sim 10^{-4}$ at these scales.

Two factors play an important role in determining the amplitude of the B -mode power spectrum induced by reionization: (i) the ionization history; and (ii) the minimum mass of the halos hosting ionizing sources. For a given minimum halo mass, early reionization scenarios increase the induced B -mode power spectrum, although such early reionization scenarios appear to be ruled out by a variety of astrophysical data. For a given reionization history, the amplitude of the B -mode power spectrum increases with the minimum mass of ionizing sources on the scales of interest. At $l \sim 100$, even relatively extreme assumptions about the ionization history or the minimum halo mass do not increase the B -mode power spectrum beyond the primary signal for $r \sim 10^{-3}$.

Near-future ground-based experiments, such as BICEP Array, Simons Observatory, and CMB-S4 [15, 104, 130], aim to have the sensitivity to detect the primary B modes around $l \sim 100$ for tensor-to-scalar ratios as low as $r \sim 10^{-3}$. For these experiments, we showed bias from not accounting for the B modes induced by patchy reionization is small. Future space missions such as LiteBIRD, PICO, and CMB-Bharat aim to target both the B -mode signals generated by homogeneous reionization ($l \lesssim 20$) as well as recombination [7, 8, 127]. Patchy reionization is a negligible contaminant to the former for detectable levels of primordial gravitational waves.

With sufficient sensitivity and aggressive delensing, future experiments may be able to reach $r < 10^{-4}$ with measurements around the recombination peak. In this case, contamination from patchy reionization could become significant and might have to be addressed in order to establish the nature of the measured signal. Marginalising over the amplitude of the patchy reionization power

spectrum should be very effective at removing any bias, albeit with a modest increase in the statistical error on r , since the *shape* of the patchy reionization power spectrum on large scales is very similar across plausible reionization models. One could also consider partially removing the B modes induced by patchy reionization in a process similar to delensing. This would additionally remove the cosmic variance of the patchy-reionization signal from the error on r . The optical depth fluctuations can be reconstructed with quadratic estimators applied to the observed CMB fields [26]. This reconstruction can be combined with the observed small-scale E -mode polarization to approximate the B modes produced by patchy screening, which can be subtracted from the observed B modes. The situation is more complicated for the B modes produced by patchy scattering since one also needs the projection on the sky of the remote temperature quadrupole anisotropy through reionization. However, this can be estimated from the large-angle E -mode polarization (e.g., from a future space mission).

In conclusion, we do not expect the search for primordial B modes will be hindered by patchy reionization in the near future. For more conventional reionization histories, all currently-planned ground-based CMB experiments should be safe from significant contamination.

Acknowledgments

AR would like to thank the Kavli Institute for Cosmology Cambridge (KICC) for hospitality during the early phases of this project. The authors would like to thank Marcelo Alvarez, Nicholas Battaglia, Tirthankar Roy Choudhury, Rishi Khatri, Cora Dvorkin, Ranjan Modak, David Spergel, and Matteo Viel for useful discussions. The results presented in the paper relied on the Cambridge Service for Data Driven Discovery (CSD3) operated by the University of Cambridge (www.csd3.cam.ac.uk), provided by Dell EMC and Intel using Tier-2 funding from the Engineering and Physical Sciences Research Council (capital grant EP/P020259/1), and DiRAC funding from the Science and Technology Facilities Council (www.dirac.ac.uk). This work further used the COSMA Data Centric system operated Durham University on behalf of the STFC DiRAC HPC Facility. This equipment was funded by a BIS National E-infrastructure capital grant ST/K00042X/1, DiRAC Operations grant ST/K003267/1 and Durham University. DiRAC is part of the National E-Infrastructure. This work is partially supported by PRIN MIUR 2015 grant ‘Cosmology and Fundamental Physics: illuminating the Dark Universe with Euclid’, PRIN INAF 2014 grant ‘Probing the AGN/galaxy co-evolution through ultra-deep and ultra-high-resolution radio surveys’, the MIUR grant ‘Finanziamento annuale individuale attivita base di ricerca’ and the RADIOFOREGROUNDS grant (COMPET-05-2015, agreement number 687312) of the European Union Horizon 2020 research and innovation program. PDM acknowledges support from a Kavli Institute Senior Fellowship at the University of Cambridge and the Netherlands organization for scientific research (NWO) VIDI grant (dossier 639.042.730). MGH, GK and AR acknowledge support from ERC Advanced Grant 320596 ‘Emergence’. AC and MH acknowledge support from the UK Science and Technology Facilities Council (grant numbers ST/N000927/1 and ST/S000623/1). While working on this paper, we learned about very similar work in preparation by Mukherjee et al. [40]. Although our simulation approach differs from theirs, we obtain similar conclusions. We have included comparison to their work in several places throughout this paper.

References

- [1] M. Kamionkowski and E. D. Kovetz, *The Quest for B Modes from Inflationary Gravitational Waves*, *Annual Review of Astronomy and Astrophysics* **54** (Sep, 2016) 227–269, [[1510.06042](https://arxiv.org/abs/1510.06042)].
- [2] H. Hui, P. A. R. Ade, Z. Ahmed, R. W. Aikin, K. D. Alexander, D. Barkats et al., *BICEP Array: a multi-frequency degree-scale CMB polarimeter*, in *Millimeter, Submillimeter, and Far-Infrared Detectors and Instrumentation for Astronomy IX*, vol. 10708 of *Society of Photo-Optical Instrumentation Engineers (SPIE) Conference Series*, p. 1070807, July, 2018, [1808.00568](https://arxiv.org/abs/1808.00568), DOI.
- [3] B. A. Benson, P. A. R. Ade, Z. Ahmed, S. W. Allen, K. Arnold, J. E. Austermann et al., *SPT-3G: a next-generation cosmic microwave background polarization experiment on the South Pole telescope*, in *Millimeter, Submillimeter, and Far-Infrared Detectors and Instrumentation for Astronomy VII*, vol. 9153 of *Proc. SPIE*, p. 91531P, July, 2014, [1407.2973](https://arxiv.org/abs/1407.2973), DOI.

- [4] P. Ade, J. Aguirre, Z. Ahmed, S. Aiola, A. Ali, D. Alonso et al., *The Simons Observatory: science goals and forecasts*, *Journal of Cosmology and Astro-Particle Physics* **2019** (Feb, 2019) 056, [[1808.07445](#)].
- [5] K. N. Abazajian, P. Adshead, Z. Ahmed, S. W. Allen, D. Alonso, K. S. Arnold et al., *CMB-S4 Science Book, First Edition, arXiv e-prints* (Oct, 2016) arXiv:1610.02743, [[1610.02743](#)].
- [6] T. Matsumura, Y. Akiba, J. Borrill, Y. Chinone, M. Dobbs, H. Fuke et al., *Mission Design of LiteBIRD*, *Journal of Low Temperature Physics* **176** (Sep, 2014) 733–740, [[1311.2847](#)].
- [7] B. M. Sutin, M. Alvarez, N. Battaglia, J. Bock, M. Bonato, J. Borrill et al., *PICO - the probe of inflation and cosmic origins*, in *Space Telescopes and Instrumentation 2018: Optical, Infrared, and Millimeter Wave*, vol. 10698 of *Society of Photo-Optical Instrumentation Engineers (SPIE) Conference Series*, p. 106984F, Jul, 2018, [[1808.01368](#), DOI].
- [8] CMB-Bharat: An Indian Cosmology Consortium, “Exploring Cosmic History and Origin: A proposal for a next generation space mission for near-ultimate measurements of the Cosmic Microwave Background (CMB) polarization and discovery of global CMB spectral distortions.” <http://cmb-bharat.in/wp-content/uploads/2018/06/cmb-bharat-rao-tp-es.pdf>, 2018.
- [9] Planck Collaboration, Y. Akrami, F. Arroja, M. Ashdown, J. Aumont, C. Baccigalupi et al., *Planck 2018 results. I. Overview and the cosmological legacy of Planck*, *arXiv e-prints* (Jul, 2018) arXiv:1807.06205, [[1807.06205](#)].
- [10] T. Louis, E. Grace, M. Hasselfield, M. Lungu, L. Maurin, G. E. Addison et al., *The Atacama Cosmology Telescope: two-season ACTPol spectra and parameters*, *Journal of Cosmology and Astro-Particle Physics* **2017** (Jun, 2017) 031, [[1610.02360](#)].
- [11] D. Hanson, S. Hoover, A. Crites, P. A. R. Ade, K. A. Aird, J. E. Austermann et al., *Detection of B-Mode Polarization in the Cosmic Microwave Background with Data from the South Pole Telescope*, *Physical Review Letters* **111** (Oct., 2013) 141301, [[1307.5830](#)].
- [12] BICEP2 and Keck Array Collaborations, P. A. R. Ade, Z. Ahmed, R. W. Aikin, K. D. Alexander, D. Barkats et al., *BICEP2/Keck Array V: Measurements of B-mode Polarization at Degree Angular Scales and 150 GHz by the Keck Array*, *ApJ* **811** (Oct, 2015) 126, [[1502.00643](#)].
- [13] BICEP2 Collaboration, Keck Array Collaboration, P. A. R. Ade, Z. Ahmed, R. W. Aikin, K. D. Alexander et al., *Constraints on Primordial Gravitational Waves Using Planck, WMAP, and New BICEP2/Keck Observations through the 2015 Season*, *Phys. Rev. Lett.* **121** (Nov, 2018) 221301, [[1810.05216](#)].
- [14] P. Creminelli, S. Dubovsky, D. López Nacir, M. Simonović, G. Trevisan, G. Villadoro et al., *Implications of the scalar tilt for the tensor-to-scalar ratio*, *Phys. Rev. D* **92** (Dec, 2015) 123528, [[1412.0678](#)].
- [15] K. N. Abazajian, P. Adshead, Z. Ahmed, S. W. Allen, D. Alonso, K. S. Arnold et al., *CMB-S4 Science Book, First Edition, ArXiv e-prints* (Oct., 2016) , [[arxiv:1610.02743](#)].
- [16] Planck Collaboration, R. Adam, P. A. R. Ade, N. Aghanim, M. Arnaud, M. Ashdown et al., *Planck 2015 results. IX. Diffuse component separation: CMB maps*, *A&A* **594** (Sep, 2016) A9, [[1502.05956](#)].
- [17] BICEP2/Keck Collaboration, Planck Collaboration, P. A. R. Ade, N. Aghanim, Z. Ahmed, R. W. Aikin et al., *Joint Analysis of BICEP2/Keck Array and Planck Data*, *Phys. Rev. Lett.* **114** (Mar, 2015) 101301, [[1502.00612](#)].
- [18] Planck Collaboration, R. Adam, P. A. R. Ade, N. Aghanim, M. Arnaud, J. Aumont et al., *Planck intermediate results. XXX. The angular power spectrum of polarized dust emission at intermediate and high Galactic latitudes*, *A&A* **586** (Feb., 2016) A133, [[1409.5738](#)].
- [19] M. Zaldarriaga and U. Seljak, *Gravitational lensing effect on cosmic microwave background polarization*, *Phys. Rev. D* **58** (July, 1998) 023003, [[astro-ph/9803150](#)].
- [20] A. Lewis and A. Challinor, *Weak gravitational lensing of the CMB*, *Phys. Rep.* **429** (June, 2006) 1–65, [[astro-ph/0601594](#)].
- [21] R. A. Sunyaev and Y. B. Zeldovich, *The Observations of Relic Radiation as a Test of the Nature of X-Ray Radiation from the Clusters of Galaxies*, *Comments on Astrophysics and Space Physics* **4** (Nov., 1972) 173.

- [22] R. A. Sunyaev and I. B. Zeldovich, *Microwave background radiation as a probe of the contemporary structure and history of the universe*, *ARA&A* **18** (1980) 537–560.
- [23] N. Y. Gnedin and A. H. Jaffe, *Secondary Cosmic Microwave Background Anisotropies from Cosmological Reionization*, *ApJ* **551** (Apr., 2001) 3–14, [[astro-ph/0008469](#)].
- [24] O. Zahn, M. Zaldarriaga, L. Hernquist and M. McQuinn, *The Influence of Nonuniform Reionization on the CMB*, *ApJ* **630** (Sept., 2005) 657–666, [[astro-ph/0503166](#)].
- [25] W. Hu, *Reionization revisited: secondary cmb anisotropies and polarization*, *Astrophys. J.* **529** (2000) 12, [[astro-ph/9907103](#)].
- [26] C. Dvorkin and K. M. Smith, *Reconstructing patchy reionization from the cosmic microwave background*, *Phys. Rev. D* **79** (Feb., 2009) 043003, [[arxiv:0812.1566](#)].
- [27] C. Dvorkin, W. Hu and K. M. Smith, *B-mode CMB polarization from patchy screening during reionization*, *Phys. Rev. D* **79** (May, 2009) 107302, [[arxiv:0902.4413](#)].
- [28] P. A. R. Ade, Y. Akiba, A. E. Anthony, K. Arnold, M. Atlas, D. Barron et al., *Measurement of the Cosmic Microwave Background Polarization Lensing Power Spectrum with the POLARBEAR Experiment*, *Physical Review Letters* **113** (July, 2014) 021301, [[1312.6646](#)].
- [29] A. van Engelen, B. D. Sherwin, N. Sehgal, G. E. Addison, R. Allison, N. Battaglia et al., *The Atacama Cosmology Telescope: Lensing of CMB Temperature and Polarization Derived from Cosmic Infrared Background Cross-correlation*, *ApJ* **808** (July, 2015) 7, [[1412.0626](#)].
- [30] Polarbear Collaboration, P. A. R. Ade, Y. Akiba, A. E. Anthony, K. Arnold, M. Atlas et al., *A Measurement of the Cosmic Microwave Background B-mode Polarization Power Spectrum at Sub-degree Scales with POLARBEAR*, *ApJ* **794** (Oct., 2014) 171, [[1403.2369](#)].
- [31] BICEP2 Collaboration, P. A. R. Ade, R. W. Aikin, D. Barkats, S. J. Benton, C. A. Bischoff et al., *Detection of B-Mode Polarization at Degree Angular Scales by BICEP2*, *Physical Review Letters* **112** (June, 2014) 241101, [[1403.3985](#)].
- [32] R. Keisler, S. Hoover, N. Harrington, J. W. Henning, P. A. R. Ade, K. A. Aird et al., *Measurements of Sub-degree B-mode Polarization in the Cosmic Microwave Background from 100 Square Degrees of SPTpol Data*, *The Astrophysical Journal* **807** (Jul, 2015) 151, [[1503.02315](#)].
- [33] M. Kesden, A. Cooray and M. Kamionkowski, *Separation of Gravitational-Wave and Cosmic-Shear Contributions to Cosmic Microwave Background Polarization*, *Physical Review Letters* **89** (July, 2002) 011304, [[astro-ph/0202434](#)].
- [34] L. Knox and Y.-S. Song, *Limit on the Detectability of the Energy Scale of Inflation*, *Physical Review Letters* **89** (July, 2002) 011303, [[astro-ph/0202286](#)].
- [35] U. Seljak and C. M. Hirata, *Gravitational lensing as a contaminant of the gravity wave signal in the CMB*, *Phys. Rev. D* **69** (Feb., 2004) 043005, [[astro-ph/0310163](#)].
- [36] N. Y. Gnedin and A. H. Jaffe, *Secondary Cosmic Microwave Background Anisotropies from Cosmological Reionization*, *ApJ* **551** (Apr., 2001) 3–14, [[astro-ph/0008469](#)].
- [37] W. Hu, *Reionization Revisited: Secondary Cosmic Microwave Background Anisotropies and Polarization*, *ApJ* **529** (Jan., 2000) 12–25, [[astro-ph/9907103](#)].
- [38] M. G. Santos, A. Cooray, Z. Haiman, L. Knox and C.-P. Ma, *Small-Scale Cosmic Microwave Background Temperature and Polarization Anisotropies Due to Patchy Reionization*, *ApJ* **598** (Dec., 2003) 756–766, [[astro-ph/0305471](#)].
- [39] A. Roy, A. Lapi, D. Spergel and C. Baccigalupi, *Observing patchy reionization with future CMB polarization experiments*, *JCAP* **5** (May, 2018) 014, [[1801.02393](#)].
- [40] S. Mukherjee, S. Paul and T. R. Choudhury, *Is patchy reionization an obstacle in detecting the primordial gravitational wave signal?*, *arXiv e-prints* (Mar, 2019) arXiv:1903.01994, [[1903.01994](#)].
- [41] C. L. Bennett, M. Halpern, G. Hinshaw, N. Jarosik, A. Kogut, M. Limon et al., *First-Year Wilkinson Microwave Anisotropy Probe (WMAP) Observations: Preliminary Maps and Basic Results*, *ApJS* **148** (Sept., 2003) 1–27, [[astro-ph/0302207](#)].

- [42] Planck Collaboration, N. Aghanim, Y. Akrami, M. Ashdown, J. Aumont, C. Baccigalupi et al., *Planck 2018 results. VI. Cosmological parameters*, *ArXiv e-prints* (July, 2018) , [[1807.06209](#)].
- [43] G. Kulkarni, G. Worseck and J. F. Hennawi, *Evolution of the AGN UV luminosity function from redshift 7.5*, *arXiv e-prints* (July, 2018) , [[1807.09774](#)].
- [44] R. J. Bouwens, G. D. Illingworth, P. A. Oesch, J. Caruana, B. Holwerda, R. Smit et al., *Reionization after Planck: The Derived Growth of the Cosmic Ionizing Emissivity now matches the Growth of the Galaxy UV Luminosity Density*, *Astrophys. J.* **811** (2015) 140, [[1503.08228](#)].
- [45] J. Chisholm, S. Gazagnes, D. Schaerer, A. Verhamme, J. R. Rigby, M. Bayliss et al., *Accurately predicting the escape fraction of ionizing photons using restframe ultraviolet absorption lines*, *ArXiv e-prints* (Mar., 2018) , [[1803.03655](#)].
- [46] J. Matthee, D. Sobral, M. Gronke, A. Paulino-Afonso, M. Stefanon and H. Röttgering, *Confirmation of double peaked Lyman-alpha emission at $z=6.593$: Witnessing a galaxy directly contributing to the reionisation of the Universe*, *ArXiv e-prints* (May, 2018) , [[1805.11621](#)].
- [47] T. J. Fletcher, B. E. Robertson, K. Nakajima, R. S. Ellis, D. P. Stark and A. Inoue, *The Lyman Continuum Escape Survey: Ionizing Radiation from [O III]-Strong Sources at a Redshift of 3.1*, *ArXiv e-prints* (June, 2018) , [[1806.01741](#)].
- [48] C. C. Steidel, M. Bogosavlevic, A. E. Shapley, N. A. Reddy, G. C. Rudie, M. Pettini et al., *The Keck Lyman Continuum Spectroscopic Survey (KLCS): The Emergent Ionizing Spectrum of Galaxies at $z \sim 3$* , *ArXiv e-prints* (May, 2018) , [[1805.06071](#)].
- [49] G. Kulkarni, T. R. Choudhury, E. Puchwein and M. G. Haehnelt, *Large 21-cm signals from AGN-dominated reionization*, *MNRAS* **469** (Aug., 2017) 4283–4291, [[1701.04408](#)].
- [50] X. Fan, M. A. Strauss, R. H. Becker, R. L. White, J. E. Gunn, G. R. Knapp et al., *Constraining the Evolution of the Ionizing Background and the Epoch of Reionization with $z \sim 6$ Quasars. II. A Sample of 19 Quasars*, *AJ* **132** (July, 2006) 117–136, [[astro-ph/0512082](#)].
- [51] G. D. Becker, J. S. Bolton, P. Madau, M. Pettini, E. V. Ryan-Weber and B. P. Venemans, *Evidence of patchy hydrogen reionization from an extreme Ly α trough below redshift six*, *MNRAS* **447** (Mar., 2015) 3402–3419, [[1407.4850](#)].
- [52] S. E. I. Bosman, X. Fan, L. Jiang, S. Reed, Y. Matsuoka, G. Becker et al., *New constraints on Lyman- α opacity with a sample of 62 quasars at $z > 5.7$* , *MNRAS* (May, 2018) , [[1802.08177](#)].
- [53] A.-C. Eilers, F. B. Davies and J. F. Hennawi, *The Opacity of the Intergalactic Medium Measured Along Quasar Sightlines at $z \sim 6$* , *ApJ* **864** (Sept., 2018) 53, [[1807.04229](#)].
- [54] G. D. Becker, F. B. Davies, S. R. Furlanetto, M. A. Malkan, E. Boera and C. Douglass, *Evidence for Large-scale Fluctuations in the Metagalactic Ionizing Background Near Redshift Six*, *ApJ* **863** (Aug., 2018) 92, [[1803.08932](#)].
- [55] G. Kulkarni, L. C. Keating, M. G. Haehnelt, S. E. I. Bosman, E. Puchwein, J. Chardin et al., *Large Lyman- α opacity fluctuations and low CMB τ in models of late reionization with large islands of neutral hydrogen extending to $z \sim 5.5$* , *Mon. Not. Roy. Astron. Soc.* **485** (2019) L24–L28, [[1809.06374](#)].
- [56] S. Furlanetto, M. Zaldarriaga and L. Hernquist, *The Growth of HII regions during reionization*, *Astrophys. J.* **613** (2004) 1–15, [[astro-ph/0403697](#)].
- [57] Planck Collaboration XVI, *Planck 2013 results. XVI. Cosmological parameters*, *A&A* **571** (Nov., 2014) A16, [[1303.5076](#)].
- [58] S. Naoz, S. Noter and R. Barkana, *The first stars in the Universe*, *MNRAS* **373** (Nov, 2006) L98–L102, [[astro-ph/0604050](#)].
- [59] R. Barkana and A. Loeb, *In the beginning: the first sources of light and the reionization of the universe*, *Phys. Rep.* **349** (July, 2001) 125–238, [[astro-ph/0010468](#)].
- [60] M. J. Mortonson and W. Hu, *The Maximum B-Mode Polarization of the Cosmic Microwave Background from Inhomogeneous Reionization*, *ApJ* **657** (Mar., 2007) 1–14, [[astro-ph/0607652](#)].
- [61] M. LoVerde and N. Afshordi, *Extended limber approximation*, *Phys. Rev. D* **78** (Dec, 2008) 123506.

- [62] D. N. Limber, *The Analysis of Counts of the Extragalactic Nebulae in Terms of a Fluctuating Density Field.*, *ApJ* **117** (Jan., 1953) 134.
- [63] P. Lemos, A. Challinor and G. Efstathiou, *The effect of Limber and flat-sky approximations on galaxy weak lensing*, *JCAP* **2017** (May, 2017) 014, [[1704.01054](#)].
- [64] M. Su, A. P. S. Yadav, M. McQuinn, J. Yoo and M. Zaldarriaga, *An Improved Forecast of Patchy Reionization Reconstruction with CMB*, *ArXiv e-prints* (June, 2011) , [[arxiv:1106.4313](#)].
- [65] M. Kamionkowski and L. Knox, *Aspects of the cosmic microwave background dipole*, *Phys. Rev. D* **67** (Mar, 2003) 063001, [[astro-ph/0210165](#)].
- [66] J. S. Bolton, E. Puchwein, D. Sijacki, M. G. Haehnelt, T.-S. Kim, A. Meiksin et al., *The Sherwood simulation suite: overview and data comparisons with the Lyman- α forest at redshifts $2 \leq z \leq 5$* , *Mon. Not. Roy. Astron. Soc.* **464** (2017) 897–914, [[1605.03462](#)].
- [67] V. Springel, N. Yoshida and S. D. M. White, *GADGET: a code for collisionless and gasdynamical cosmological simulations*, *New Astron.* **6** (Apr., 2001) 79–117, [[astro-ph/0003162](#)].
- [68] V. Springel, *The cosmological simulation code GADGET-2*, *MNRAS* **364** (Dec., 2005) 1105–1134, [[astro-ph/0505010](#)].
- [69] M. Viel, M. G. Haehnelt and V. Springel, *Inferring the dark matter power spectrum from the Lyman α forest in high-resolution QSO absorption spectra*, *MNRAS* **354** (Nov., 2004) 684–694, [[astro-ph/0404600](#)].
- [70] A. H. Pawlik, J. Schaye and E. van Scherpenzeel, *Keeping the Universe ionized: photoheating and the clumping factor of the high-redshift intergalactic medium*, *MNRAS* **394** (Apr., 2009) 1812–1824, [[0807.3963](#)].
- [71] J. Chardin, G. Kulkarni and M. G. Haehnelt, *Self-shielding of hydrogen in the IGM during the epoch of reionization*, *MNRAS* **478** (July, 2018) 1065–1076, [[1707.06993](#)].
- [72] F. Haardt and P. Madau, *Radiative Transfer in a Clumpy Universe. IV. New Synthesis Models of the Cosmic UV/X-Ray Background*, *ApJ* **746** (Feb., 2012) 125, [[1105.2039](#)].
- [73] G. D. Becker, J. S. Bolton, M. G. Haehnelt and W. L. W. Sargent, *Detection of extended He II reionization in the temperature evolution of the intergalactic medium*, *MNRAS* **410** (Jan., 2011) 1096–1112, [[1008.2622](#)].
- [74] J. Oñorbe, F. B. Davies, Z. Lukić, J. F. Hennawi and D. Sorini, *Inhomogeneous Reionization Models in Cosmological Hydrodynamical Simulations*, *arXiv e-prints* (Oct, 2018) arXiv:1810.11683, [[1810.11683](#)].
- [75] G. Kulkarni, J. F. Hennawi, J. Oñorbe, A. Rorai and V. Springel, *Characterizing the Pressure Smoothing Scale of the Intergalactic Medium*, *ApJ* **812** (Oct., 2015) 30, [[1504.00366](#)].
- [76] J. Oñorbe, J. F. Hennawi and Z. Lukić, *Self-consistent Modeling of Reionization in Cosmological Hydrodynamical Simulations*, *ApJ* **837** (Mar., 2017) 106, [[1607.04218](#)].
- [77] N. Katz, D. H. Weinberg and L. Hernquist, *Cosmological Simulations with TreeSPH*, *ApJS* **105** (July, 1996) 19, [[astro-ph/9509107](#)].
- [78] S. Ikeuchi and J. P. Ostriker, *Evolution of the intergalactic medium - What happened during the epoch $Z = 3-10?$* , *ApJ* **301** (Feb., 1986) 522–543.
- [79] D. Aubert and R. Teyssier, *A radiative transfer scheme for cosmological reionization based on a local Eddington tensor*, *MNRAS* **387** (June, 2008) 295–307, [[0709.1544](#)].
- [80] D. Aubert and R. Teyssier, *Reionization Simulations Powered by Graphics Processing Units. I. On the Structure of the Ultraviolet Radiation Field*, *ApJ* **724** (Nov., 2010) 244–266, [[1004.2503](#)].
- [81] L. C. Keating, E. Puchwein and M. G. Haehnelt, *Spatial fluctuations of the intergalactic temperature-density relation after hydrogen reionization*, *MNRAS* **477** (July, 2018) 5501–5516, [[1709.05351](#)].
- [82] B. Greig, A. Mesinger, Z. Haiman and R. A. Simcoe, *Are we witnessing the epoch of reionisation at $z = 7.1$ from the spectrum of J1120+0641?*, *MNRAS* **466** (Apr., 2017) 4239–4249, [[1606.00441](#)].

- [83] F. B. Davies, J. F. Hennawi, E. Bañados, Z. Lukić, R. Decarli, X. Fan et al., *Quantitative Constraints on the Reionization History from the IGM Damping Wing Signature in Two Quasars at $z \gtrsim 7$* , *ApJ* **864** (Sep, 2018) 142, [[1802.06066](#)].
- [84] I. McGreer, A. Mesinger and V. D’Odorico, *Model-independent evidence in favour of an end to reionization by $z \approx 6$* , *Mon. Not. Roy. Astron. Soc.* **447** (2015) 499–505, [[1411.5375](#)].
- [85] A. Lapi, C. Mancuso, A. Celotti and L. Danese, *Galaxy Evolution at High Redshift: Obscured Star Formation, GRB Rates, Cosmic Reionization, and Missing Satellites*, *ApJ* **835** (Jan., 2017) 37, [[arxiv:1612.01304](#)].
- [86] G. Worseck, J. X. Prochaska, J. F. Hennawi and M. McQuinn, *Early and Extended Helium Reionization over More Than 600 Million Years of Cosmic Time*, *ApJ* **825** (July, 2016) 144, [[1405.7405](#)].
- [87] G. Worseck, F. B. Davies, J. F. Hennawi and J. X. Prochaska, *The Evolution of the HeII-Ionizing Background at Redshifts $2.3 \lesssim z \lesssim 3.8$ Inferred from a Statistical Sample of 24 HST/COS HeII Ly α Absorption Spectra*, *Astrophys. J.* **875** (2019) 111, [[1808.05247](#)].
- [88] A. Mesinger, S. Furlanetto and R. Cen, *21CMFAST: a fast, seminumerical simulation of the high-redshift 21-cm signal*, *MNRAS* **411** (Feb., 2011) 955–972, [[1003.3878](#)].
- [89] A. Mesinger and S. Furlanetto, *Efficient Simulations of Early Structure Formation and Reionization*, *ApJ* **669** (Nov., 2007) 663–675, [[0704.0946](#)].
- [90] Y. B. Zel’Dovich, *Reprint of 1970A&A.....5...84Z. Gravitational instability: an approximate theory for large density perturbations.*, *A&A* **500** (Mar, 2070) 13–18.
- [91] G. Efstathiou, M. Davis, S. D. M. White and C. S. Frenk, *Numerical techniques for large cosmological N -body simulations*, *ApJS* **57** (Feb, 1985) 241–260.
- [92] F. B. Davies, G. D. Becker and S. R. Furlanetto, *Determining the Nature of Late Gunn-Peterson Troughs with Galaxy Surveys*, *ApJ* **860** (Jun, 2018) 155, [[1708.08927](#)].
- [93] F. B. Davies, S. R. Furlanetto and K. L. Dixon, *A self-consistent 3D model of fluctuations in the helium-ionizing background*, *MNRAS* **465** (Mar, 2017) 2886–2894, [[1703.10177](#)].
- [94] M. G. Santos, L. Ferramacho, M. B. Silva, A. Amblard and A. Cooray, *Fast large volume simulations of the 21-cm signal from the reionization and pre-reionization epochs*, *MNRAS* **406** (Aug, 2010) 2421–2432, [[0911.2219](#)].
- [95] C. Lacey and S. Cole, *Merger rates in hierarchical models of galaxy formation*, *MNRAS* **262** (June, 1993) 627–649.
- [96] J. R. Bond, S. Cole, G. Efstathiou and N. Kaiser, *Excursion set mass functions for hierarchical Gaussian fluctuations*, *ApJ* **379** (Oct., 1991) 440–460.
- [97] S. R. Furlanetto, M. Zaldarriaga and L. Hernquist, *Statistical Probes of Reionization with 21 Centimeter Tomography*, *ApJ* **613** (Sept., 2004) 16–22, [[astro-ph/0404112](#)].
- [98] T. R. Choudhury, M. G. Haehnelt and J. Regan, *Inside-out or outside-in: the topology of reionization in the photon-starved regime suggested by Ly α forest data*, *MNRAS* **394** (Apr., 2009) 960–977, [[0806.1524](#)].
- [99] A. Mesinger, S. Furlanetto and R. Cen, *21CMFAST: a fast, seminumerical simulation of the high-redshift 21-cm signal*, *MNRAS* **411** (Feb., 2011) 955–972, [[1003.3878](#)].
- [100] G. Kulkarni, T. R. Choudhury, E. Puchwein and M. G. Haehnelt, *Models of the cosmological 21 cm signal from the epoch of reionization calibrated with Ly α and CMB data*, *MNRAS* **463** (Dec., 2016) 2583–2599, [[1607.03891](#)].
- [101] S. R. Furlanetto, M. Zaldarriaga and L. Hernquist, *The Growth of H II Regions During Reionization*, *ApJ* **613** (Sept., 2004) 1–15, [[astro-ph/0403697](#)].
- [102] O. Zahn, A. Lidz, M. McQuinn, S. Dutta, L. Hernquist, M. Zaldarriaga et al., *Simulations and Analytic Calculations of Bubble Growth during Hydrogen Reionization*, *ApJ* **654** (Jan., 2007) 12–26, [[astro-ph/0604177](#)].

- [103] L. Knox, *Determination of inflationary observables by cosmic microwave background anisotropy experiments*, *Phys. Rev. D* **52** (Oct, 1995) 4307–4318, [[astro-ph/9504054](#)].
- [104] The Simons Observatory Collaboration, P. Ade, J. Aguirre, Z. Ahmed, S. Aiola, A. Ali et al., *The Simons Observatory: Science goals and forecasts*, *ArXiv e-prints* (Aug., 2018) , [[1808.07445](#)].
- [105] K. Abazajian, G. Addison, P. Adshead, Z. Ahmed, S. W. Allen, D. Alonso et al., *CMB-S4 Science Case, Reference Design, and Project Plan*, *arXiv e-prints* (Jul, 2019) arXiv:1907.04473, [[1907.04473](#)].
- [106] M. Hazumi et al., *Litebird: A satellite for the studies of b-mode polarization and inflation from cosmic background radiation detection*, *Journal of Low Temperature Physics* **194** (Mar, 2019) 443–452.
- [107] S. Hanany, M. Alvarez, E. Artis, P. Ashton, J. Aumont, R. Aurlien et al., *PICO: Probe of Inflation and Cosmic Origins*, *arXiv e-prints* (Feb, 2019) arXiv:1902.10541, [[1902.10541](#)].
- [108] S. W. Henderson, R. Allison, J. Austermann, T. Baildon, N. Battaglia, J. A. Beall et al., *Advanced ACTPol Cryogenic Detector Arrays and Readout*, *Journal of Low Temperature Physics* **184** (Aug, 2016) 772–779, [[1510.02809](#)].
- [109] Z. Ahmed, M. Amiri, S. J. Benton, J. J. Bock, R. Bowens-Rubin, I. Buder et al., *BICEP3: a 95GHz refracting telescope for degree-scale CMB polarization*, in *Millimeter, Submillimeter, and Far-Infrared Detectors and Instrumentation for Astronomy VII*, vol. 9153 of Proc. SPIE, p. 91531N, Aug., 2014, [1407.5928](#), DOI.
- [110] A. Suzuki, P. Ade, Y. Akiba, C. Aleman, K. Arnold, C. Baccigalupi et al., *The Polarbear-2 and the Simons Array Experiments*, *Journal of Low Temperature Physics* **184** (Aug., 2016) 805–810, [[1512.07299](#)].
- [111] X. Wang and W. Hu, *Redshift Space 21 cm Power Spectra from Reionization*, *ApJ* **643** (June, 2006) 585–597, [[astro-ph/0511141](#)].
- [112] POLARBEAR Collaboration, P. A. R. Ade, M. Aguilar, Y. Akiba, K. Arnold, C. Baccigalupi et al., *A Measurement of the Cosmic Microwave Background B-mode Polarization Power Spectrum at Subdegree Scales from Two Years of polarbear Data*, *The Astrophysical Journal* **848** (Oct, 2017) 121, [[1705.02907](#)].
- [113] A. Lewis, *Cosmological parameters from WMAP 5-year temperature maps*, *Phys. Rev.* **D78** (2008) 023002, [[0804.3865](#)].
- [114] S. Dumitru, G. Kulkarni, G. Lagache and M. G. Haehnelt, *Predictions and sensitivity forecasts for reionization-era [C II] line intensity mapping*, *MNRAS* **485** (May, 2019) 3486–3498, [[1802.04804](#)].
- [115] L. C. Keating, L. H. Weinberger, G. Kulkarni, M. G. Haehnelt, J. Chardin and D. Aubert, *Long troughs in the Lyman- α forest below redshift 6 due to islands of neutral hydrogen*, *arXiv e-prints* (May, 2019) arXiv:1905.12640, [[1905.12640](#)].
- [116] E. Vanzella et al., *The Great Observatories Origins Deep Survey: Constraints on the Lyman Continuum Escape Fraction Distribution of Lyman-Break Galaxies at $3.4 < z < 4.5$* , *Astrophys. J.* **725** (2010) 1011–1031, [[1009.1140](#)].
- [117] J. Chisholm, S. Gazagnes, D. Schaerer, A. Verhamme, J. R. Rigby, M. Bayliss et al., *Accurately predicting the escape fraction of ionizing photons using rest-frame ultraviolet absorption lines*, *A&A* **616** (Aug, 2018) A30, [[1803.03655](#)].
- [118] C. C. Steidel, M. Bogosavljević, A. E. Shapley, N. A. Reddy, G. C. Rudie, M. Pettini et al., *The Keck Lyman Continuum Spectroscopic Survey (KLCS): The Emergent Ionizing Spectrum of Galaxies at $z \sim 3$* , *ApJ* **869** (Dec, 2018) 123, [[1805.06071](#)].
- [119] J. Japelj, E. Vanzella, F. Fontanot, S. Cristiani, G. B. Caminha, P. Tozzi et al., *Constraints on the Lyman continuum escape fraction for faint star-forming galaxies*, *MNRAS* **468** (June, 2017) 389–403, [[1612.06401](#)].
- [120] A. E. Shapley, C. C. Steidel, A. L. Strom, M. Bogosavljević, N. A. Reddy, B. Siana et al., *Q1549-C25: A Clean Source of Lyman-Continuum Emission at $z = 3.15$* , *ApJ* **826** (Aug., 2016) L24, [[1606.00443](#)].
- [121] R. E. Mostardi, A. E. Shapley, C. C. Steidel, R. F. Trainor, N. A. Reddy and B. Siana, *A High-Resolution Hubble Space Telescope Study of Apparent Lyman Continuum Leakers at $z \sim 3$* , *ApJ* **810** (Sept., 2015) 107, [[1506.08201](#)].

- [122] S. Borthakur, T. M. Heckman, C. Leitherer and R. A. Overzier, *A local clue to the reionization of the universe*, *Science* **346** (Oct., 2014) 216–219, [[1410.3511](#)].
- [123] A. Grazian, E. Giallongo, R. Gerbasi, F. Fiore, A. Fontana, O. Le Fèvre et al., *The Lyman continuum escape fraction of galaxies at $z = 3.3$ in the VUDS-LBC/COSMOS field*, *A&A* **585** (Jan., 2016) A48, [[1509.01101](#)].
- [124] Y. I. Izotov, I. Orlitová, D. Schaerer, T. X. Thuan, A. Verhamme, N. G. Guseva et al., *Eight per cent leakage of Lyman continuum photons from a compact, star-forming dwarf galaxy*, *Nature* **529** (Jan., 2016) 178–180, [[1601.03068](#)].
- [125] Y. I. Izotov, G. Worseck, D. Schaerer, N. G. Guseva, T. X. Thuan, V. Fricke, A. et al., *Low-redshift Lyman continuum leaking galaxies with high $[O\ III]/[O\ II]$ ratios*, *MNRAS* **478** (Aug., 2018) 4851–4865, [[1805.09865](#)].
- [126] Y. I. Izotov, D. Schaerer, G. Worseck, N. G. Guseva, T. X. Thuan, A. Verhamme et al., *J1154+2443: a low-redshift compact star-forming galaxy with a 46 per cent leakage of Lyman continuum photons*, *MNRAS* **474** (Mar., 2018) 4514–4527, [[1711.11449](#)].
- [127] Y. Sekimoto, P. Ade, K. Arnold, J. Aumont, J. Austermann, C. Baccigalupi et al., *Concept design of the LiteBIRD satellite for CMB B-mode polarization*, in *Space Telescopes and Instrumentation 2018: Optical, Infrared, and Millimeter Wave*, vol. 10698 of *Society of Photo-Optical Instrumentation Engineers (SPIE) Conference Series*, p. 106981Y, Aug., 2018, [DOI](#).
- [128] J. Errard, S. M. Feeney, H. V. Peiris and A. H. Jaffe, *Robust forecasts on fundamental physics from the foreground-obscured, gravitationally-lensed CMB polarization*, *JCAP* **2016** (Mar, 2016) 052, [[1509.06770](#)].
- [129] N. Krachmalnicoff, C. Baccigalupi, J. Aumont, M. Bersanelli and A. Mennella, *Characterization of foreground emission on degree angular scales for CMB B-mode observations . Thermal dust and synchrotron signal from Planck and WMAP data*, *A&A* **588** (Apr., 2016) A65, [[1511.00532](#)].
- [130] H. Hui, P. A. R. Ade, Z. Ahmed, R. W. Aikin, K. D. Alexander, D. Barkats et al., *BICEP Array: a multi-frequency degree-scale CMB polarimeter*, in *Proc. SPIE*, vol. 10708 of *Society of Photo-Optical Instrumentation Engineers (SPIE) Conference Series*, p. 1070807, July, 2018, [1808.00568](#), [DOI](#).